Department of Electrical
and
Computer Systems Engineering

Technical Report
MECSE-11-2005

Photonic Signal Processing - Part II.1: Dispersion Compensation Processors

L. N. Binh

MONASH
UNIVERSITY

PHOTONIC SIGNAL PROCESSING - PART II.1:

DISPERSION COMPENSATION PROCESSORS

Le Nguyen Binh

Laboratory for Optical Communications and Applied Photonics, Department of Electrical and Computer Systems Engineering, Monash University, Clayton Victoria 3168 Australia

e-mail le.nguyen.binh@eng.monash.edu.au

Abstract

Dispersion compensating device finds very important role in advanced optical transmission systems due to its simplicity and potential uses in several locations of the system. This report outlines the synthesis and performance of a photonic circuit that would compensate the linear induced dispersion in the fibre link.

The compensator, a double coupler doubly resonator, composed of two optical couplers and interconnecting and feedback paths is synthesised using the photonic signal flow graph technique and the discrete z-transform. The frequency and phase responses of the photonic circuit, are obtained and hence their dispersion characteristics at the edges of the resonator. The pole-zero patterns of the compensator are examined so as to design the dispersion factor which is required to be in opposite sign and equal to that of the transmission fibre. The compensator is then used to equalise the induced fibre dispersion in an optical transmission system. The eye diagram evaluation proves the superiority of the photonic compensator.

CONTENTS

TABLE OF FIGURES

1 INTRODUCTION

Optical fiber communication has progressed tremendously over the last few decades. The transmission distance has reached from few hundred kms to few thousand kms of standard single mode optical fibres (SSMF) and non-zero-dispersion shifted fibres (NZ-DSF). This is possible with the employment of dispersion management technique by which the dispersion of the transmission path is compensated by the same amount of dispersion but in opposite sign. Dispersion compensation thus becomes very important in advanced optically amplified communications systems.

On the other hand photonic signal processing (PSP) is becoming more and more popular due to its ability of processing the lightwave modulated signals and representation of lightwaves in discrete domain. This report gives applications of PSP technique in the design of photonic processors for dispersion compensating of transmitted lightwave signals in optical fiber communication systems. The synthesis of such photonic circuit by the use of the z-domain representation is presented for the photonic signals flow in the photonic processor, a double coupler doubly resonant circuit as shown in *Figure 1*. We then obtain the optical transfer function in discrete domain and then the phase, group delay and hence dispersion and dispersion slope of the compensator. These compensators are used for compensation of an optical transmission system using SSMF as the transmission medium. It has been proven that the eye diagram of the PRBS sequence is remarkably improved and error free can be achieved.

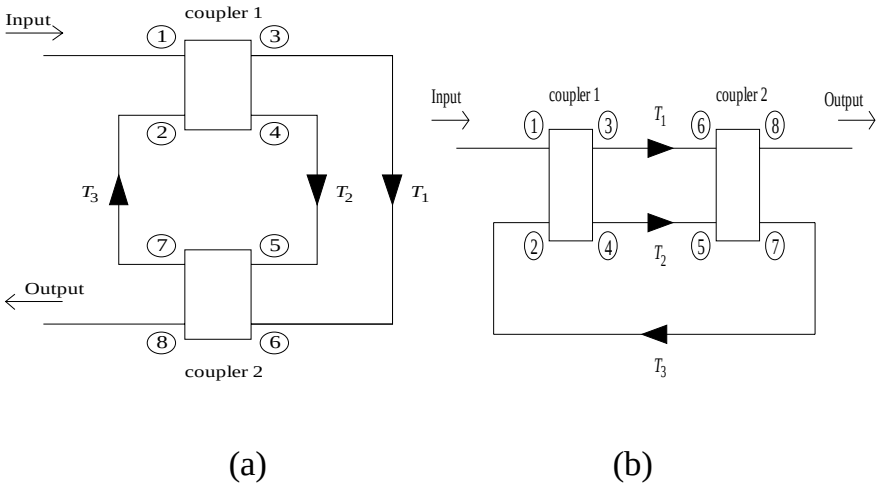

Figure 1 (a) Schematic diagram of the DCDR circuit, (b) the same circuit in alternate arrangement. Numbers in circle indicate Port order. All lines are optical transmission line of either fibres or integrated optic waveguides – amplified or non-amplified.

The report is organised as follows: Section 2 gives details of the design of the compensator including a graphical technique and the frequency and phase responses. Section 3 then describe the optical transmission systems and the performance of the compensator. Finally concluding remarks are stated.

2 DCDR PHOTONIC CIRCUIT UNDER COHERENT SOURCE OPERATION

This section presents the resonance effect of the DCDR circuit which can be analysed using the field representation. The circuit is excited by coherent source with finite very narrow linewidth. The DCDR circuit is considered as a resonator here rather than as a recirculating delay line. Previous studies on the effect of source coherence on the performance of resonator circuit are included reference [2.1-2.6], but the analysis on DCDR circuit has not been reported. Using our newly developed SFG theory [2.8] for photonic circuits, these difficulties can be overcome easily. In this section, an algorithm using the Z-transform representation, its transfer unction and amplitude and phase responses are described. The temporal transient response of the circuit shown with source coherence is also reported.

2.1 Field analysis of the DCDR circuit

Before considering the case for source with finite linewidth, we first derive the transfer functions of the DCDR circuit in terms of the optical field. The analysis in this section is different from the preceding intensity-basis analysis in the sense that the phase change encountered by the signal in the circuit would be taken into consideration, thus interferometric effects can take place. Therefore, the resonance effect of the DCDR circuit can be investigated as shown in *Figure 2*. Typical signal flow diagrams can be obtained as shown in *Figure 2* and *Figure 3*. We define the DCDR circuit parameters in the field regime in terms of the parameters. The circuit parameters are defined as : $k_{pcf} = -j\sqrt{k_p}$ where p = 1,2 as the field cross-coupling coefficient for the two couplers, $k_{pdf} = \sqrt{1-k_p}$ where p = 1,2 as the field direct-coupling coefficient for the two couplers 1 and 2 and $T_{if} = \sqrt{t_{ai}G_i}\,z^{-m_i}$ for i = 1,2 and 3. The j term in the k_{pcf} expression above accounts for the $-\pi/2$ phase shift induced by the coupler during the cross-coupling.

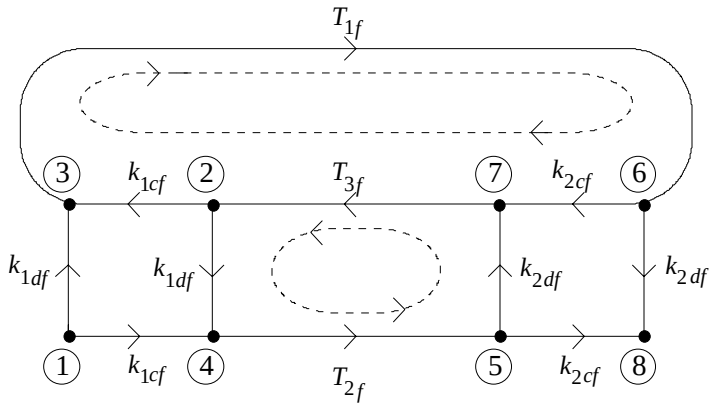

Figure 2 SFG of the DCDR circuit in terms of the field variables

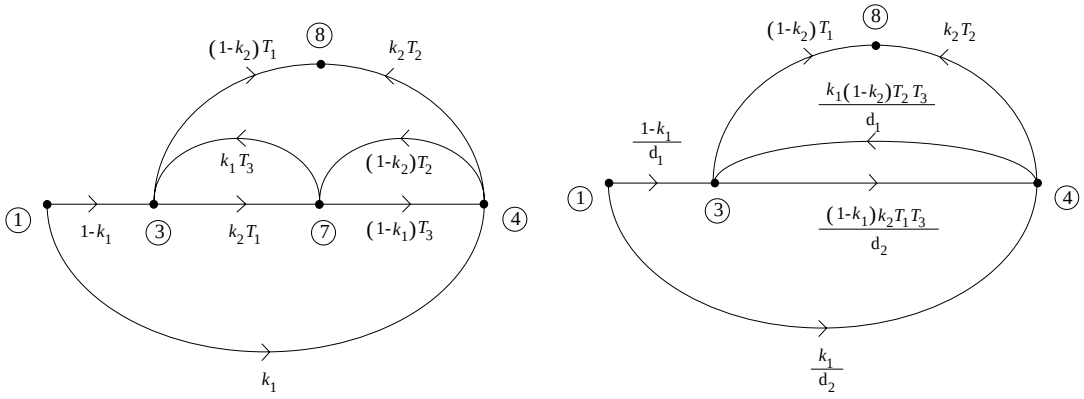

Figure 3 Simplified SFGs of Figure 2 of the DCDR circuit (a) First reduction, and (b) second reduction.

2.2 Output-input field transfer function

The output-input field transfer function of the DCDR circuit, by application of the optical Mason's Rule is given by [3.15]:

$$H_{18f} = \frac{E_8}{E_1} = \frac{\sum_{q=1}^{4} F_{qf}\Delta_{qf}}{\Delta_f} \tag{1}$$

E_8 and E_1 are the output and input field amplitude respectively of the DCDR circuit. The loop transmittances and the forward path transmittances can be obtained as follows:

2.2.1(a) Loop transmittances

(i) Loop 1 : (2)(3)(6)(7)(2): The loop optical transmittance of Loop 1 (in terms of lightwave field) is

$$T_{l1f} = k_{1cf} k_{2cf} T_{1f} T_{3f}, \quad (2)$$

(ii) Loop 2: (2)(4)(5)(7)(2): Optical transmittance of Loop 2:

$$T_{l2f} = k_{1df} k_{2df} T_{2f} T_{3f}. \quad (3)$$

2.2.2(b) Forward path transmittances

The four forward paths and their related transmittances are:

Path 1: connecting nodes (1)(3)(6)(8)

$$F_{1f} = k_{1df} k_{2df} T_{1f}, \quad (4)$$

$$\Delta_{1f} = 1\text{-}T_{l2f}. \quad (5)$$

Path 2: connecting nodes (1)(3)(6)(7)(2)(4)(5)(8)

$$F_{2f} = k_{1df}{}^{2} k_{2cf}{}^{2} T_{1f} T_{2f} T_{3f}, \quad (6)$$

$$\Delta_{2f} = 1. \quad (7)$$

Δ_{2f} is equal to unity due to its forward path touching both optical loops.

Path 3: connecting nodes (1)(4)(5)(7)(2)(3)(6)(8)

$$F_{3f} = k_{1cf}{}^{2} k_{2df}{}^{2} T_{1f} T_{2f} T_{3f}, \quad (8)$$

$$\Delta_{3f} = 1. \quad (9)$$

Δ_{3f} is equal to unity due to the touching of two loops of the forward path.

Path 4: connecting nodes (1)(4)(5)(8)

$$F_{4f} = k_{1cf} k_{2cf} T_{2f}, \tag{10}$$

$$\Delta_{4f} = 1\text{-}T_{l1f}. \tag{11}$$

Also, the loop determinant Δ_f is given by

$$\Delta_f = 1 - T_{l1f} - T_{l2f} \tag{12}$$

The output-input field transfer function is thus expressed as, from (1):

$$H_{18f} = \frac{\sqrt{(1-k_1)(1-k_2)}T_{1f} - \sqrt{k_1 k_2}T_{2f} - T_{1f}T_{2f}T_{3f}}{1+\sqrt{k_1 k_2}T_{1f}T_{3f} - \sqrt{(1-k_1)(1-k_2)}T_{2f}T_{3f}} \tag{13}$$

which is in terms of k_1, k_2, T_{1f}, T_{2f} and T_{3f}

2.3 Circulating-input field transfer functions

Similarly the circulating-input field transfer functions can be derived similarly as above and is given as

$$H_{13f} = \frac{\sqrt{(1-k_1)} - \sqrt{(1-k_2)}T_{2f}T_{3f}}{DEN_f} \tag{14}$$

$$H_{14f} = \frac{-j\sqrt{k_1} - j\sqrt{k_2}T_{1f}T_{3f}}{DEN_f} \tag{15}$$

$$H_{17f} = \frac{-j\sqrt{k_1(1-k_2)}T_{2f} - j\sqrt{(1-k_1)k_2}T_{1f}}{DEN_f} \tag{16}$$

where $DEN_f = 1+\sqrt{k_1k_2}T_{1f}T_{3f} - \sqrt{(1-k_1)(1-k_2)}T_{2f}T_{3f}$ (17)

2.4 Resonance condition

The usual definition of optical resonance in a photonic circuit is that at a particular frequency or wavelength the optical output is at a minimum while the optical energy is circulating in the loops of the photonic circuit. Thus the resonant condition can be found by setting the output transfer function to zero or effectively finding the zeroes of the output-input optical transfer function. In this case, the DCDR circuit can be referred as a resonator. Consider (11), if $t_{a1} = t_{a2} = t_{a3} = t_a$, $k_1 = k_2 = k$, $G_1 = G_2 = G_3 = 1$ and $m_1 = m_2 = m_3 = 1$, the equation can be simplified to

$$H_{18f} = \frac{(1-2k)\sqrt{t_a}z^{-1} - t_a\sqrt{t_a}z^{-3}}{1-(1-2k)t_az^{-2}} \quad (18)$$

Rearranging (18) gives

$$H_{18f} = \frac{(1-2k)\sqrt{t_a}z^{2} - t_a\sqrt{t_a}}{z^{3}-(1-2k)t_az} \quad (19)$$

2.4.1Condition

Setting the numerator in (18) to zero resulting in two resonance conditions:

(i) if $z^2 = -1$, $k = (1+t_a)/2$ (20)

(ii) if $z^2 = 1$, $k = (1-t_a)/2$ (21)

$z^2 = -1$ means $z = \pm j$ which can be interpreted as $\omega\tau = n\pi - \pi/2$, $n = 1,2...$. Recall that $\omega\tau$ is the phase change through a fibre path in the circuit with unit delay time. Similarly, $z^2 = 1$ which means $z = \pm 1$ and it can be interpreted as $\omega\tau = n\pi$, $n = 1, 2...$. As t_a is close to one for low-loss fibres, k for resonance would be close to one and zero respectively for the two resonant conditions in eqns. (20) and (21).

By inspecting the signal-flow-graph of the DCDR circuit in *Figure 2*, it can be seen that there are two touching loops. Loop1 and Loop 2 are indicated by paths (2)(3)(6)(7)(2)and(2)(4)(5)(7)(2) with their loop transmittances given by (2) and (3) respectively. Thence equations (20) and (21) are the resonant

conditions of the Loop 1 and Loop 2 respectively. The frequency response of the output-input intensity transfer function and the circulating-input intensity transfer functions under the resonant conditions given in (20) and (21) are plotted in *Figure 4* and *Figure 7* respectively. The instantaneous optical intensities are obtained by taking the square of the modulus of the corresponding field amplitudes. The vertical scale of the magnitude plot is shown with the absolute magnitude.

2.4.2Pole-zero pattern, frequency and impulse responses

Figure 5 and Figure 6 illustrate two more conditions for operating the photonic processor including their pole and zero patterns to indicate the resonance conditions or non-resonance. The setting parameters are shown in Table 1.

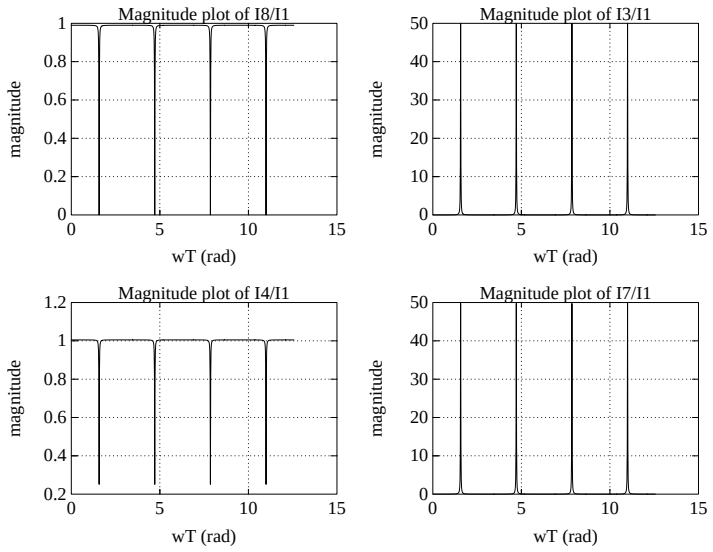

Figure 4 Frequency response of the output-input intensity transfer function and the circulating-input intensity transfer functions of the DCDR resonator under the resonant conditions of t_a = 0.99 and k = 0.995 which satisfy the condition listed in (20).

	k_1	k_2	poles	zeros
Fig. 3.5	0.9	0.9	0, ±0.905539	±0.883452
Fig. 3.6	0.2	0.8	0, ±0.565685	±j1.06066
Fig. 3.7	0.5	0.5	0, ±0.707107	0, 0

Table 1 Circuit parameters used in the analysis of the passive DCDR response with the corresponding poles and zeros of the output-input intensity transfer function H_{18}.

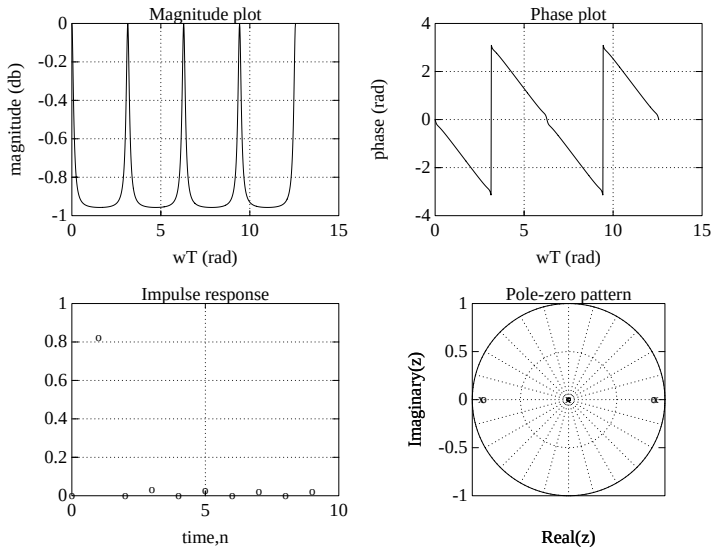

Figure 5 Frequency response, impulse response and pole-zero plot (pole: x, zero: o) for the passive (non-amplified) DCDR circuit with circuit parameters given in Table 1

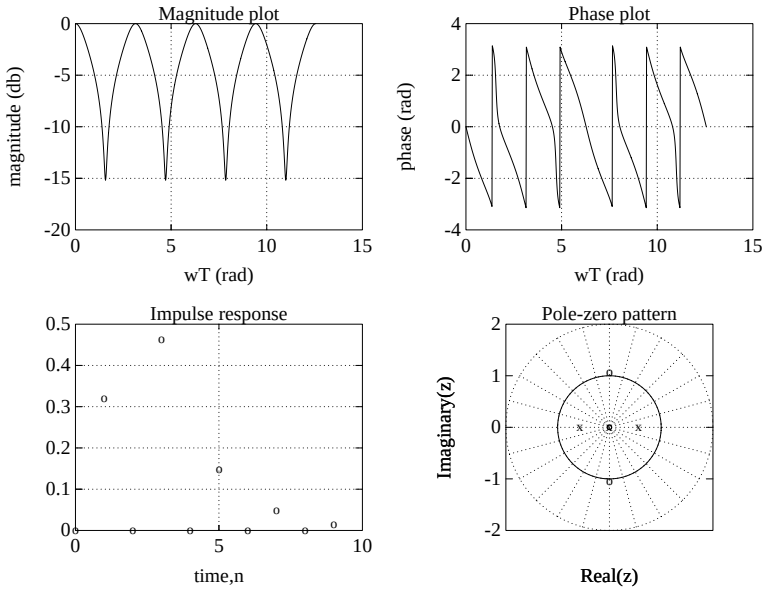

Figure 6 Frequency response, impulse response and pole-zero plots for the passive DCDR circuit with circuit parameters as given in Table 1.

In *Figure 4*, there are maximums for the circulating intensity I_3 at $\omega\tau = \pi/2, 3\pi/2, 5\pi/2$ and $7\pi/2$ and correspondingly there are minimums for the output intensity I_8 and circulating intensity I_4 at these

positions. This shows the resonance of Loop 1 of the DCDR resonator. Indeed the resonance criterion on the phase change for the signal in the circuit is that the round-loop phase change of the resonant loop needed to be $2n\pi$ where n is an integer. Inspecting the criterion on $\omega\tau$ (the phase change per fibre path with unit delay) for resonance of Loop 1 in (20), it shows the above point. The round-loop phase change for Loop 1 in this case is $2(n\pi - \pi/2)$ plus the phase change encountered across the couplers which is $\pi/2$ per coupler. It is obvious that this sum adds up to the value of $2n\pi$. This is another way of inspecting the resonance condition; hence it can be determined by just examining the circuit's signal flow graph. The resonance of Loop 2 of the DCDR resonator is shown in *Figure 7*. The maximums for the circulating intensity I_4 are located at $\omega\tau = \pi, 2\pi, 3\pi$ and 4π and correspondingly the minimums for the output intensity I_8 and circulating intensity I_4 at these positions.

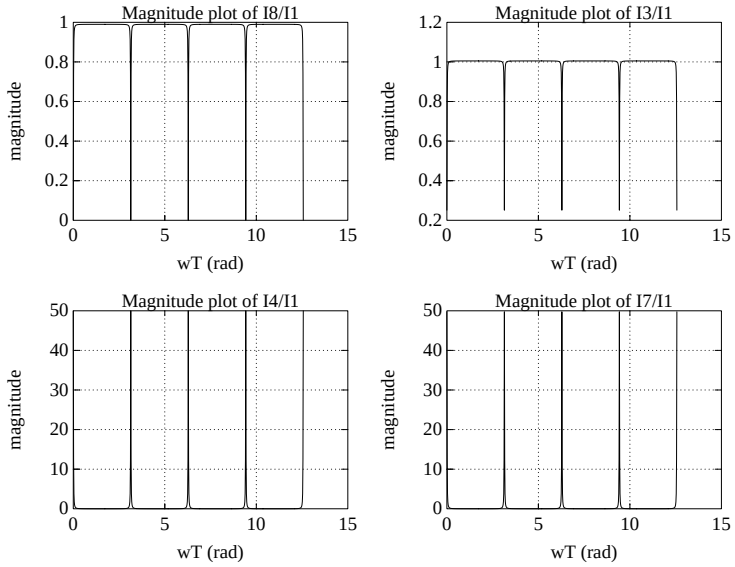

Figure 7 Frequency response of the output-input intensity transfer function and the circulating-input intensity transfer functions of the DCDR resonator under the resonant conditions of t_a = 0.99 and k = 0.005 which satisfy the condition listed in (21).

It is also found that the sharpness (or arrow bandwidth) of the resonance depends on the circuit parameters. In *Figure 8*, resonance behaviour of the DCDR resonator is shown with t_a = 0.8 and k = 0.1 which corresponds to the resonance of Loop 2 of the resonator. A smaller value of t_a is used here which indicates the loss in the fibre path is larger. It is clearly seen that the maximum value of the circulating intensity I_4 is much smaller than the one in *Figure 7*. Thus, in this case, it can be stated that low-loss fibres should be used in building up the resonator in order to have sharp resonant peaks.

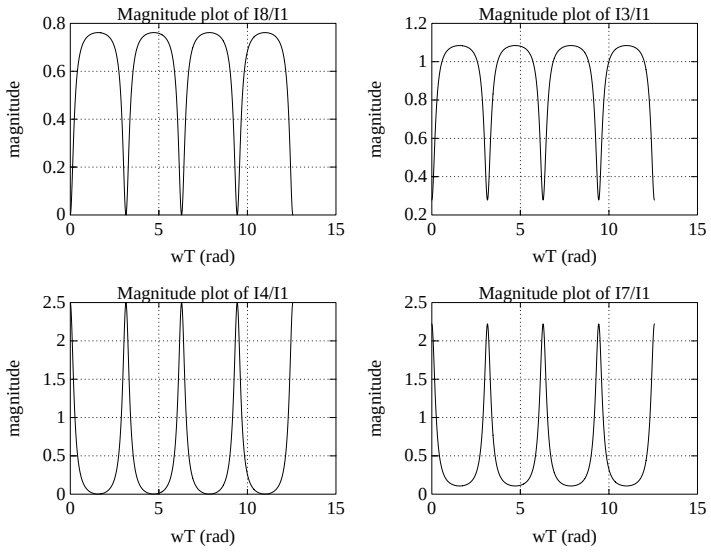

Figure 8 Frequency response of the output-input intensity transfer function and the circulating-input intensity transfer functions of the DCDR resonator under the resonant conditions of t_a = 0.8 and k = 0.1 which satisfy the condition listed in (21).

It is also observed that the energy can be stored in either of the two loops of the DCDR resonator depending on the circuit parameters. It is also noticed from *Figure 4* and *Figure 7* that H_{17f} has maximums in both cases.

2.4.3Stability condition

We can now examine the stability of the circuit under the above resonant condition. Applying Jury's Stability Test to H_{18f} in (19) results in the stability condition of

$$| (1-2k)t_a | < 1 \qquad (22)$$

Hence a stable operation of the passive DCDR resonator is always fulfilled provided that $0 < k < 1$ and $0 < t_a < 1$. If the DCDR resonator is operating in a different condition, for instance $G_1 > 1$ or $k_1 \neq k_2$, there would be other sets of resonant conditions for the resonator.

2.5 Optically amplified DCDR circuit

2.5.1 $G_1 > 1$: One optical amplifier in forward path

We investigate here the case where only one optical amplifier is inserted in the DCDR circuit and it is inserted in the path connecting between ports 3 and 6, one of the two forward paths. The output-input intensity transfer function H_{18} simplifies to

$$H_{18} = \frac{\left[(1-k_1)(1-k_2)G_1 + k_1k_2\right]z^{-1} - (1-2k_1)(1-2k_2)G_1z^{-3}}{1-\left[k_1k_2G_1 + (1-k_1)(1-k_2)\right]z^{-2}} \qquad (23)$$

the zeroes of H_{18} are thus located at

$$z_Z(1,2) = \pm\sqrt{\frac{(1-2k_1)(1-2k_2)G_1}{(1-k_1)(1-k_2)G_1 + k_1k_2}} \qquad (24)$$

The stability condition now becomes:

$$| k_1k_2G_1 + (1\tilde{-}k_1)(1\tilde{-}k_2) | < 1 \qquad (25)$$

The pole values of the output intensity transfer function H_{18} and its zero values are plotted against G_1 with different values of k_1 and k_2 as shown in *Figure 9*(a) - (c) with different values of k_1 and k_2 as indicated.

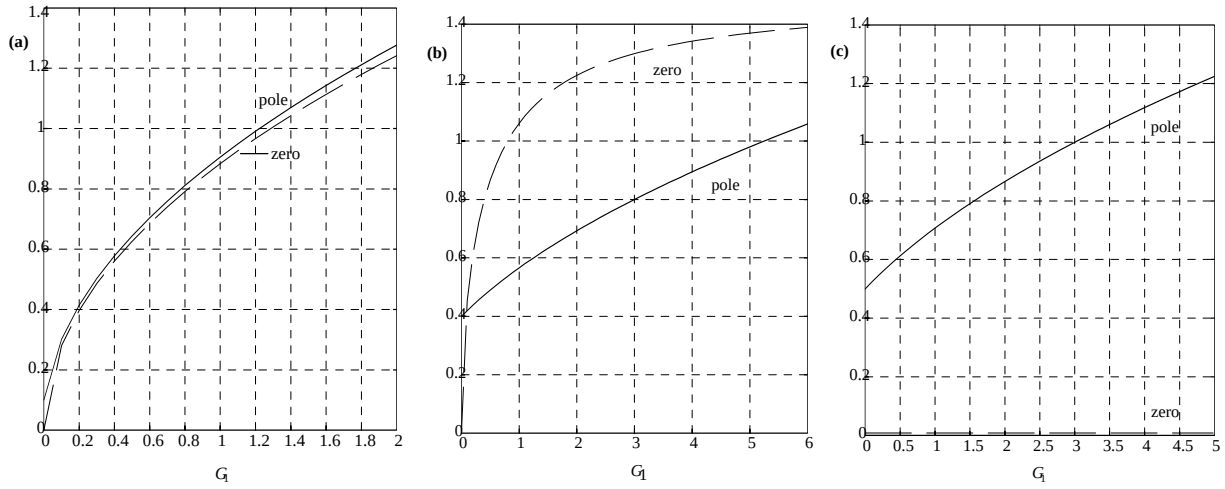

(a) (b) (c)

Figure 9 Plot of absolute magnitudes of the pole and zero of H_{18} against G_1 in case 1(b)(i). (a) $k_1 = 0.9$ and $k_2 = 0.9$, (b) $k_1 = 0.2$ and $k_2 = 0.8$, (c) $k_1 = 0.5$ and $k_2 = 0.5$.

To get a pole value close to one and just inside the unit circle, the value of G_1 needs to be 1.2, 5.2 and 3 respectively in the cases shown in *Figure 9*(a)-(c). These give us sharper frequency response or sharp roll off of the passband than its passive counterpart as are displayed in *Figure 10*(a)-(c). The data for the three figures are listed in *Table 2*.

	k_1	k_2	G_1	poles	zeros
Figure 10(a)	0.9	0.9	1.2	0, ±0.990959	±0.966595
Figure 10(b)	0.2	0.8	5.2	0, ±0.995992	±j1.373716
Figure 10(c)	0.5	0.5	3.0	0, ±1	0, 0

Table 2 Circuit parameters used in the analysis of the DCDR response with the corresponding poles and zeros of H_{18}.

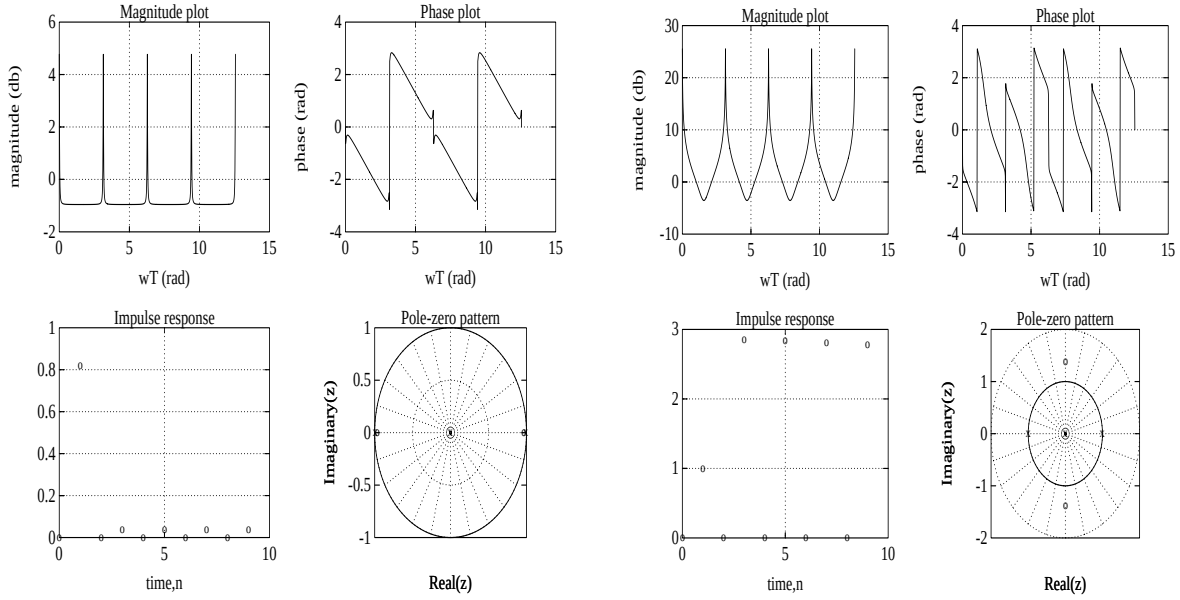

(a) (b)

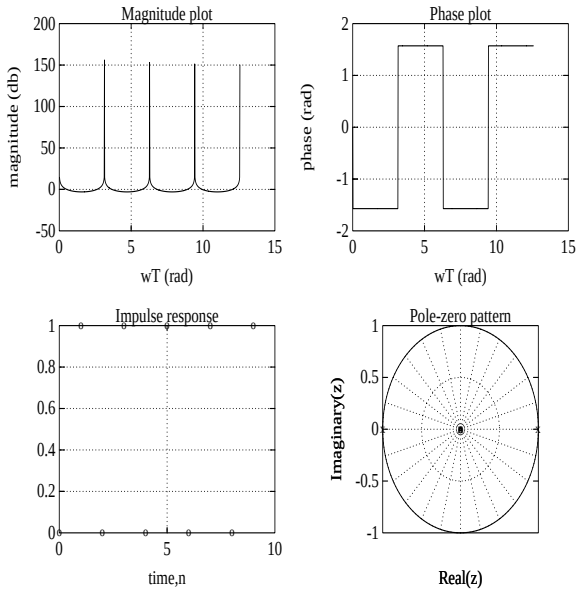

(c)

Figure 10 Frequency response, impulse response and pole-zero plots for the active DCDR circuit with circuit parameters given in (a) top row Table 2; (b) middle row Table 2 and (c) bottom row of Table 2.

Comparing *Figure 10* with *Figure 8*, the introduction of optical amplifier in the DCDR circuit enhances the performance especially the frequency response. As the pole pairs are pushed very close to the unit circle in the z-plane, it results in sharper response in the magnitude plot. Recall that the pole-zero patterns in the z-plane would play a major part in the sharpness of the resonance peak of photonic circuits. To get a sharper maximum in this particular situation, it requires that the distance between the pole and the unit circle must be less than that between the zero and the unit circle. The effect of this active mode operation can be noted by realizing that the peaks in the magnitude plot have values greater than 0dB, while in the passive operation the corresponding peaks can only come up to 0dB. This operation can be used as a band-pass filter with narrow passband.

Inspecting *Figure 10*, it is noticed that the large amplifier gain has changed the response dramatically, since its presence changes the pole-zero pattern significantly. We have a system with a pole at 0, a pole pair at ± 1 and zeros at 0 realized by the DCDR circuit. This yields a magnitude plot with very sharp peaks. The lossless system also produces an infinite constant-value impulse response. The impulse response here can be applied to generate continuous sequences of '1' pulses in signal processing system. In other words, a single impulse fed into the circuit can trigger a continuous stream of impulses of the same magnitude at the output. The causes of '0' in between the ones in the impulse response can

be understood by inspecting the geometry of the circuit. As can be seen, the consecutive output signals can only be detected every two sampling times which is the round loop time in this case. Thus, if we want to get a stream of '1' signals, we need to acquire the output every two sampling times. If not, we would get '0"1"0"1"0"1'..... .

Another application is found with the impulse response generated by the DCDR circuit. We examine the pulse response as shown in *Figure 11*(a)-(f) for input sequences consisting of '1' and '0'. For *Figure 11*(a), the steady state value of the pulse response is oscillating between 1 and 0 for an input stream with one '1'. For *Figure 11*(b), the steady state value of the pulse response is oscillating between 1 and 1 for an input stream with two '1'. In *Figure 11*(c), the steady state value of the pulse response is oscillating between 2 and 1 for an input stream with three '1'. In *Figure 11*(d), the steady state value of the pulse response is oscillating between 1 and 2 for an input stream with three '1'. Following the above pattern, we can observe that from the steady state magnitude of the pulse response, the number of '1' in the input stream can be detected. It is shown in *Figure 11*(e) and (f) for longer input streams. If we look at the stream as sequence of two-digit binary numbers, from the response we can indeed determine the occurrence of '1' in a certain digit position. For instance, in *Figure 11*(d), the input streams are '1 1' and '0 1'. The output stream in this case shows one in the first digit position and two in the second digit position which corresponds to the occurrence of '1' at that positions. The response in fact counts the numbers of '1' at the two digit positions and this may be used as an adder. This ability of counting arises from the geometry of the circuit and the orders of delay in each path. In *Figure 11*(g), $m_1 = m_2 = 3$, the circuit can count numbers of '1' in four-digit numbers as expected.

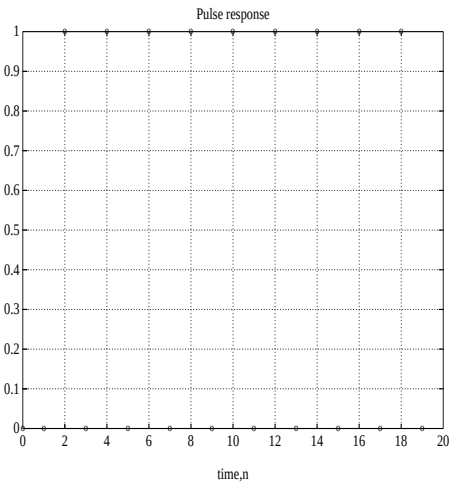

(a)

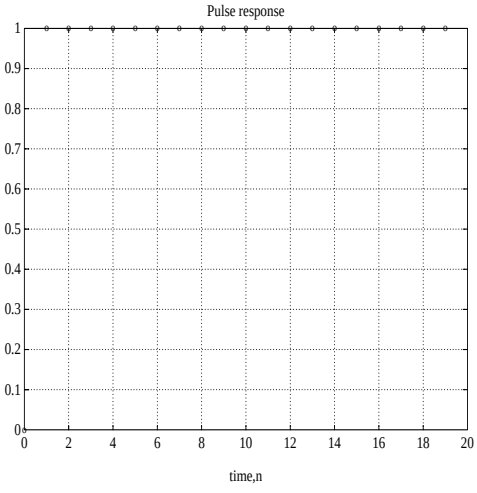

(b)

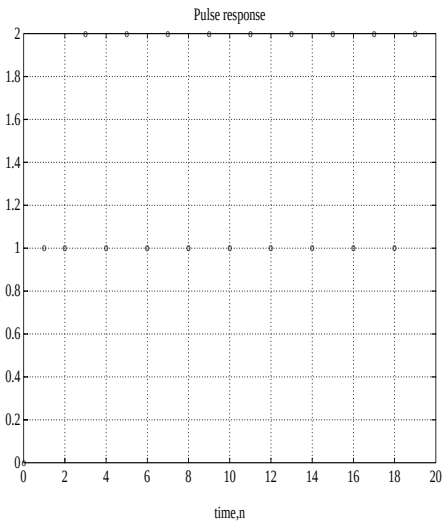

(c)

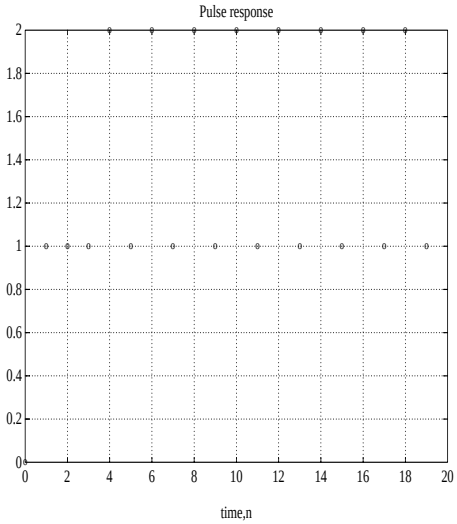

(d)

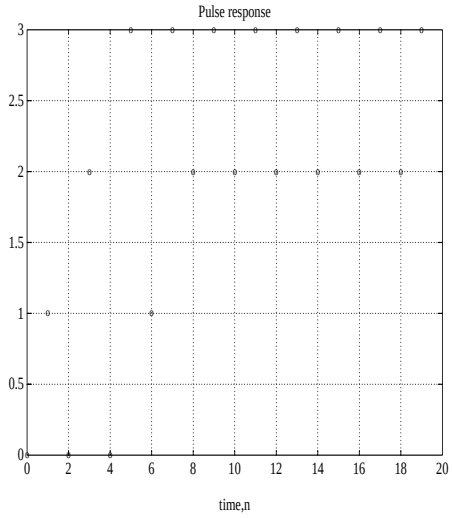

(e)

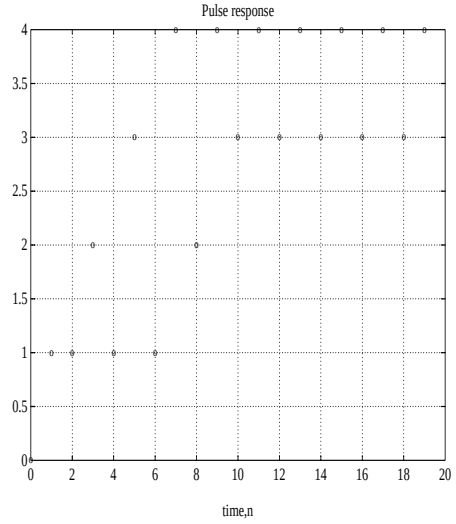

(f)

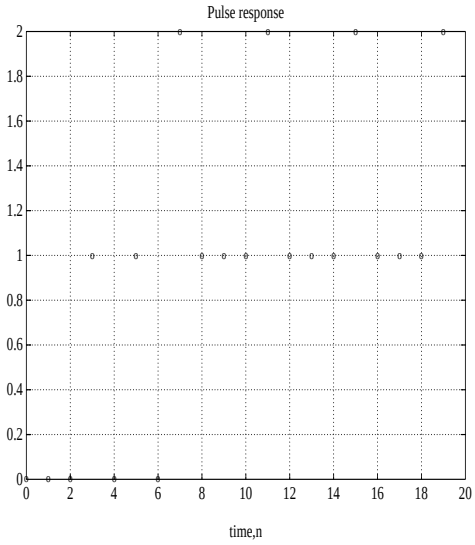

(g)

Figure 11 Pulse response of the DCDR circuit for different input sequence with $k_1 = k_2 = 0.5$, $G_1 = 3$, $G_2 = G_3 = 1$ and $m_1 = m_2 = m_3 = 1$ except (g) which has $m_1 = m_2 = 3$ and $m_3 = 1$. Input sequences for the figures (a) [0 1], (b) [1 1], (c) [1 1 1], (d) [1 1 0 1], (e) [1 0 1 0 1 1 0 1], (f) [1 1 1 0 1 0 1 1 0 1], (g) [1 0 1 0 1 1 0 1].

2.5.2 $G_2 > 1$ Optical amplifier in the other feed forward path

This case would be similar to the previous case where only one optical amplifier is placed in the other feed-forward path. The output-input intensity H_{18} becomes

$$H_{18} = \frac{\left[(1-k_1)(1-k_2)+k_1k_2G_2\right]z^{-1} - (1-2k_1)(1-2k_2)G_2z^{-3}}{1-\left[k_1k_2+(1-k_1)(1-k_2)G_2\right]z^{-2}} \qquad (26)$$

with the zeros located at:

$$z_{z(1,2)} = \pm\sqrt{\frac{(1-2k_1)(1-2k_2)G_2}{(1-k_1)(1-k_2)+k_1k_2G_2}} \qquad (27)$$

The characteristic equation remains similar to that of eqn (23) except that the coupling coefficients are interchanged and G_2 is placed appropriately.

Applying the Jury's Stability Test again we obtain the stability condition as:

$$| k_1k_2 + (1-k_1)(1-k_2)G_2 | < 1 \qquad (28)$$

The responses of the DCDR circuit in this case are similar to case 1(b)(i) which has the amplifier inserted in the other forward path of the circuit. To illustrate the duality of the two cases we try $k_1 = k_2 = 0.1$, $G_1 = 1$, $G_2 = 1.2$ and $G_3 = 1$. The circuit responses are shown to be the same of that in *Figure 9* for case 1(b)(i) where $k_1 = k_2 = 0.9$, $G_1 = 1.2$, $G_2 = G_3 = 1$, since the values of poles and zeros are the same for these two sets of parameters.

2.5.3 $G_3 > 1$ Optical amplifier in the feedback path

The output intensity transfer function H_{18} now becomes:

$$H_{18} = \frac{\left[(1-k_1)(1-k_2)+k_1k_2\right]z^{-1} - (1-2k_1)(1-2k_2)G_3z^{-3}}{1-\left[k_1k_2+(1-k_1)(1-k_2)\right]G_3z^{-2}} \qquad (29)$$

with the zeros located in the z-plane at:

$$z_Z(1,2) = \pm\sqrt{\frac{(1-2k_1)(1-2k_2)G_3}{(1-k_1)(1-k_2)+k_1k_2}} \qquad (30)$$

The stability condition follows immediately as:

$$| k_1k_2G_3 + (1\tilde{-}k_1)(1\tilde{-}k_2)G_3 | < 1 \qquad (31)$$

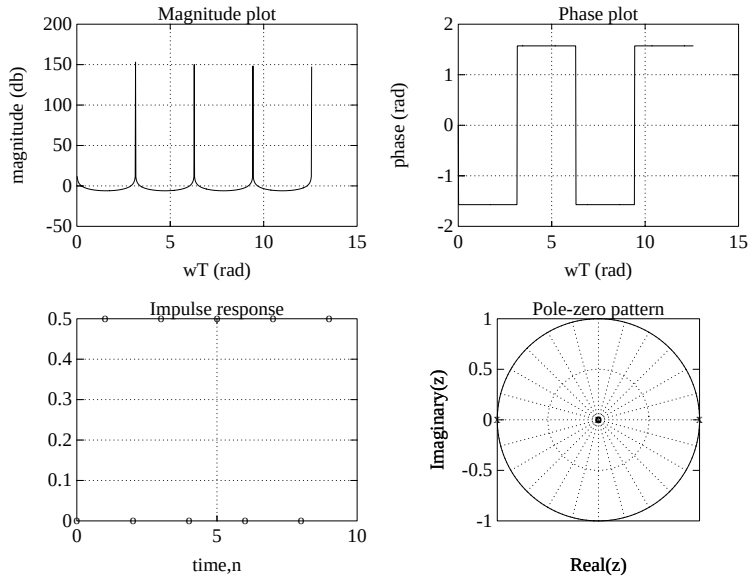

Figure 12 Frequency response, impulse response and pole-zero plot for the optically amplified DCDR circuit with $k_1 = k_2 = 0.5$, $G_1 = G_2 = 1$ and $G_3 = 2$.

In the special case of $k_1 = k_2 = 0.5$, $G_1 = G_2 = 1$ and $G_3 = 2$, the output intensity responses are plotted in *Figure 12*. With the optical amplifier situated at the feedback path rather than the feed forward path of the circuit, the optical gain required in the former case (to have the same pole and zero patterns and satisfying the stability condition) is less than that in the latter one. This makes one think to put the amplifier in the feedback path instead of putting it in the feed forward path. Nevertheless, the amplitude of the impulse response is smaller in this case where we put the amplifier in the feedback path.

The three cases for optically amplified paths have been studied where only one optical amplifier is available for the DCDR circuit. In fact, this is very important in practice when several DCDR circuits are integrated to form a network then the least number of optical amplifiers in the loop is required. Therefore, the most important question remained to be addressed is where should we place the optical amplifier in the DCDR circuit? In the feedforward or feedback path? The answer depends on specific applications.

Considering the case where the DCDR circuit is applicable as a filter then the optical amplifier should be placed in the shunt feedback path. As stated above, the amplifier in the feedback path require less optical gain than that in the feed forward path to achieve the same performance. From another point of view, we can say that with an amplifier of a particular gain, better performance would be achieved (as far as the use as a filter is concerned) if we put it in the feedback path (providing that the stability criterion is met).

If we are interested in the impulse response for applications in photonic digital processing systems, the position of the optical amplifier is very important. Also, depending on the output ports where signals are tapped, the optical amplifier must be closed to that port. Thus both cases where the optical amplifier is placed in feed-forward or feedback paths can be used for novel applications such as a dispersion compensator.

2.6 Transient response of the DCDR circuit

In Section 2.2, the frequency response of the DCDR circuit is obtained under the steady-state condition. In the following analysis, the effect of the source coherence is taken into account in evaluating the transient response of the DCDR circuit. Considering the electric field of the input light source which is expressed in the form:

$$E_1(t) = E_S(t) \exp (j(\omega_0 t + \phi(t)) , \qquad (32)$$

where $E_S(t)$ is the amplitude of the electric field at time t, ω_0 is the frequency of the source and $\phi(t)$ is the time dependent phase which represents the phase fluctuation. This is often called the phase noise in optical fiber systems[2.3]. This phase fluctuation is the cause of broadening of the optical source spectrum which results in finite linewidth of the source spectrum. We assume the source amplitude is stabilised, thus it is a linear time-invariant (LTIV) source. The light source described by (23) would then be fed into the optical circuit. Therefore, the next step is the study of the transfer function of the photonic LTIV circuit.

Here, we revisit some of the basic properties of the z-transform. Using the z-transform definition given in (1), the output-input field transfer function of the circuit H_{18f} = $H(z)$ can be stated in the form:

$$H(z) = \sum_{n=-\infty}^{\infty} h[n] z^{-n}$$

$$= \ldots + h[-1]z^{1} + h[0] + h[1]z^{-1} + h[2]z^{-2} + h[3]z^{-3} + \ldots \qquad (33)$$

An inverse z-transform manipulation would convert H_{18f} (eqn (13)) from the z-domain to the time domain. For m_1 = m_2 = m_3 = 1, that is, there is unity delay in each path of the DCDR circuit and $t_{a1} = t_{a2} = t_{a3} = 1$, the expansion of equation (13) gives:

$h[n] = 0$ for $n < 0$,

$h[0] = 0$, $h[1] = (\sqrt{(1-k_1)(1-k_2)G_1} - \sqrt{k_1 k_2 G_2})$; $h[2] = 0$;

$h[3] = -\left[\sqrt{k_1 k_2 (1-k_1)(1-k_2) G_3}(G_1 + G_2) + (k_1 + k_2 - 2k_1 k_2)\sqrt{G_1 G_2 G_3}\right]$;

and so on……. (34)

Hence, the value of $h[n]$ in (25) is the magnitude of the impulse response of the system at time index n. This is actually what we have done in previous chapters to calculate the impulse response of the circuit. Although (25) is calculated for the restricted condition m_1 = m_2 = m_3 = 1 and $t_{a1} = t_{a2} = t_{a3} = 1$ for simplicity, the following analysis is applicable to the general situation.

To compute the output of the resonator for an arbitrary input sequence (or pulse shape) $x[n]$, we perform the convolution in the time domain between $h[n]$ and $x[n]$, i.e. the output $y[n]$ is given by :

$$y[n] = h[n] * x[n] \tag{35}$$

where $*$ represents the convolution. Recall that the basic delay time of the circuit is denoted as τ and it is the sampling time as well. At time $t_n = n\tau$, the time averaged output intensity $I(t_n)$ of the DCDR circuit is

$$\langle I_8(t_n) \rangle = \langle E_8(t_n)E_8^*(t_n) \rangle \tag{36}$$

where $E_8^*(t_n)$ is the complex conjugate of $E_8(t_n)$. The angular brackets denote ensemble average. Aternatively $E_8(t_n)$ as the output at time $t_n = n\tau$ can be considered as the n^{th} sampled vaue and similarly, the input $E_1(t_n)$ at time $t_n = n\tau$ can be regarded as the n^{th} sampled input magnitude. So the former term is $y[n]$ and the latter term corresponds to $x[n]$ of (26). We can see the relationship between the discrete-time signal representation and the signals in the photonic circuit.

We now consider the effect of source coherence. In order to include the source coherence contribution to our analysis, the phase fluctuation term $exp(j\phi(t))$ of the light source as given in (23) is needed to be examined. This time-varying phase fluctuates randomly and is statistical in nature, thus statistical method is used to handle it. Traditionally, it is treated as random signal or process, and it is best described by its correlation function. This function has been determined by several authors in their papers [2.1-2.6]. In general, we consider the autocorrelation function $R[(p-s)\tau]$ of the input optical wave field and it is given as [2.2]

$$R[(p-s)\tau] = \frac{\left\langle E_1(t-p\tau)E_1^*(t-s\tau)\right\rangle}{\left[E_s(t-p\tau)E_s^*(t-s\tau)\right]} \tag{37}$$

where p and s are integers. From (23), it becomes:

$$R[(p-s)\tau] = \exp\{j[(s-p)\omega_0\tau]\}\langle \exp[j\phi(t-p\tau)]\exp[-j\phi(t-s\tau)] \rangle \tag{38}$$

If the spectrum broadening of the laser due to the random phase fluctuation $\phi(t)$ is of the Lorentzian form, the phase function $\exp[j\phi(t)]$ would have the following correlation [1,2] :

$$\langle \exp[j\phi(t-p\tau)]\exp[-j\phi(t-s\tau)] \rangle = \exp(-|s-p|\Delta\omega\tau) \quad (39)$$

where $\Delta\omega/2\pi$ is the half-width at half-maximum of the Lorentzian spectrum. Also note that $\exp(-\Delta\omega\tau)$ is the Fourier transform of the Lorentzian profile. It is related to the autocorrelation function for the phase.

Since the coherence time τ_c of the light source is equal to[2.3] :

$$\tau_c = \frac{1}{2\Delta\omega} \quad (40)$$

Thus, (40) can be rewritten as

$$\langle \exp[j\phi(t - p\tau)]\exp[-j\phi(t - s\tau)] \rangle = \exp(-|s- p|\tau/2\tau_c) \quad (41)$$

which is the same expression as obtained in Ref [2.2, 2.5]. Hence, (41) can be rewritten as

$$R[(p-s)\tau] = \exp\{ j[(s-p)\omega_0\tau]\}\exp(?|s- p|\tau/2\tau_c) \quad (42)$$

or $$R[(p-s)\tau] = \exp\{ j[(s-p)\omega_0\tau]\}D^{|s- p|} \quad (43)$$

where $D = \exp(-\tau/2\tau_c)$. This gives an expression for the phase autocorrelation function in terms of the source coherence time.

When computing $\langle I_8(t_n) \rangle$ in equation (29), products of the input field such as $\langle E_1(t_n)E_1^*(t_n) \rangle$, $\langle E_1(t_n)E_1^*(t_n-\tau) \rangle$, ... , $\langle E_1(t_n-p\tau)E_1^*(t_n-s\tau) \rangle$, ... etc. are involved as $E_8(t)$ is related to $E_1(t)$ by (28). By using eqns. (27) and (32), the values of the above products and hence $\langle I_8(t_n) \rangle$ can be found.

The general algorithms of computing the transient response of the photonic circuit are: (i) From the transfer function $H(z)$ of the optical circuit, obtain the impulse response or indeed the sequence $h[n]$ ((24).); (ii) Convolute the impulse response obtained in step 1 with the input sequence to obtain the output of the system for the pulse input ((26)); (iii) Obtain the expression for the phase fluctuation of the input, i.e. the correlation between values of phases at different times (see (28) and (33)); and (iv) Compute the output intensity of the resonator ((29)) by using result obtained in step (ii) in combination with expression in step (iii).

Therefore, using equations (25), (26), (27), (28) and (33),we can compute the transient response of the photonic circuit. The program is a general one which can compute the transient response of any photonic circuit with transfer function $H(z)$. The program has been checked with the results obtained in Ref.[2.2] for a single loop resonator and consistency is obtained. The results for the DCDR circuit are presented in the next section.

2.7 Transient responses

It can be seen from (33) that the transient response of the circuit mainly depends on the ratio of the basic time delay to the source coherence time. For the two extreme case, monochromatic source (very long coherence time, $\tau_c >> \tau$) and temporal incoherent source (very short coherence time, $\tau_c << \tau$), the value of D is equal to 1 and 0 respectively. Hence the range of D is [0, 1]. In general, the temporal response with monochromatic source is called the steady state response. The transient response corresponds to the case where the source contains finite linewidth.

Some results are shown in *Figure 13* and *Figure 14* for the passive DCDR circuit with unit delay in each path. In *Figure 13*, the circuit parameters satisfying the resonant condition (19) is used with t_a = 0.99, k = 0.995 and $\omega_o\tau$ is chosen to be $\pi/2$. The input pulse is shown in *Figure 13*(a) where the output intensity response is shown in *Figure 13*(b)-(d) with different degrees of source coherence. It is interesting to look at the incoherent case in *Figure 13*(d) in which the output is constant. In *Figure 14*, the circuit response to other input sequence (or in other words, the pulse shape) is examined. It is found in *Figure 14* that the responses for different source coherence are similar.

(a) (b)

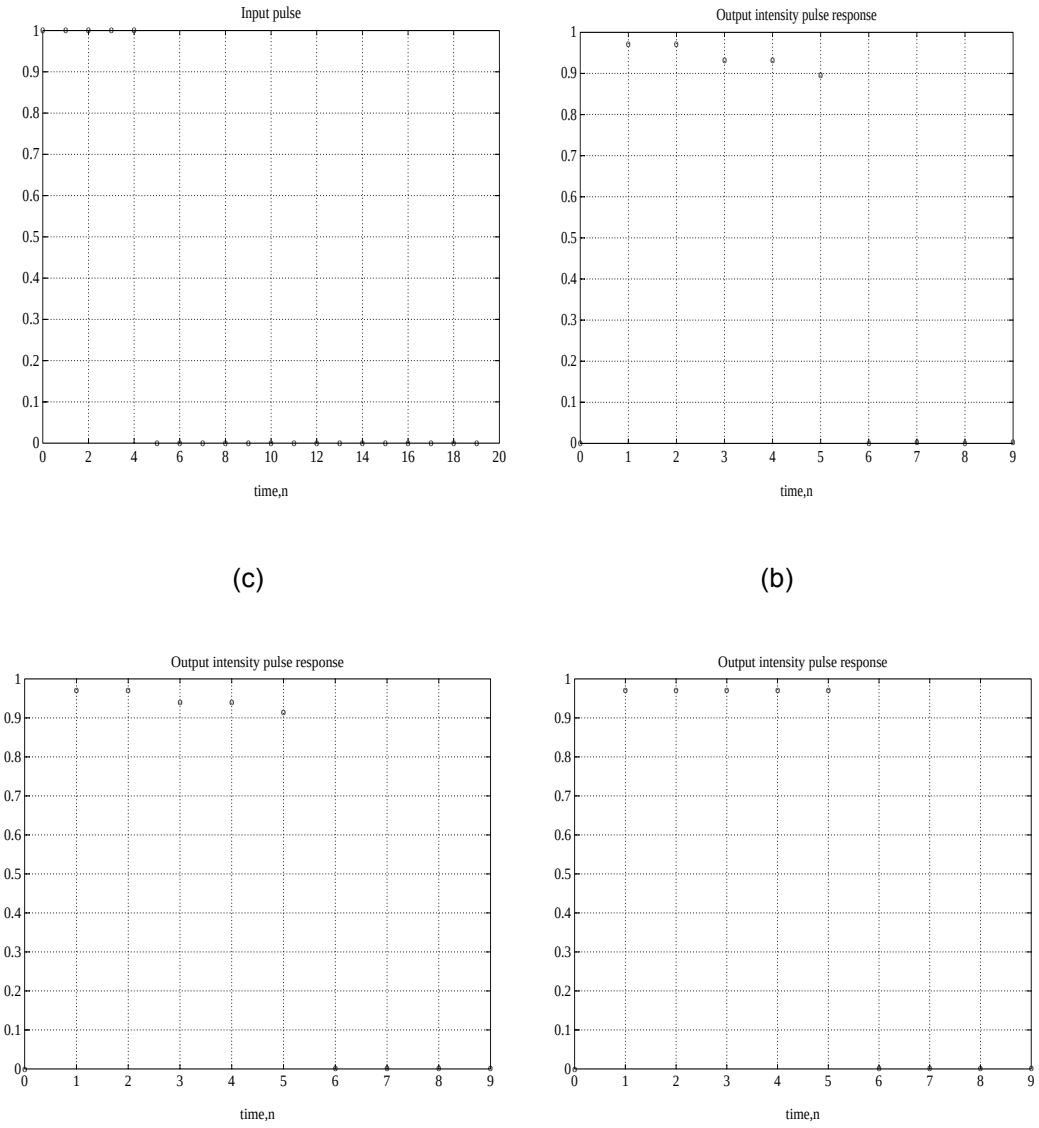

Figure 13 Transient response of the passive DCDR circuit with t_a = 0.99, k = 0.995 and $\omega_o \tau = \pi/2$. (a) Input pulse (b) Output intensity pulse with τ/τ_c = 0.001 (monochromatic) (c) Output intensity pulse with τ/τ_c = 0.2; and (d) Output intensity pulse with τ/τ_c = 500 (temporal incoherent)

(a) (b)

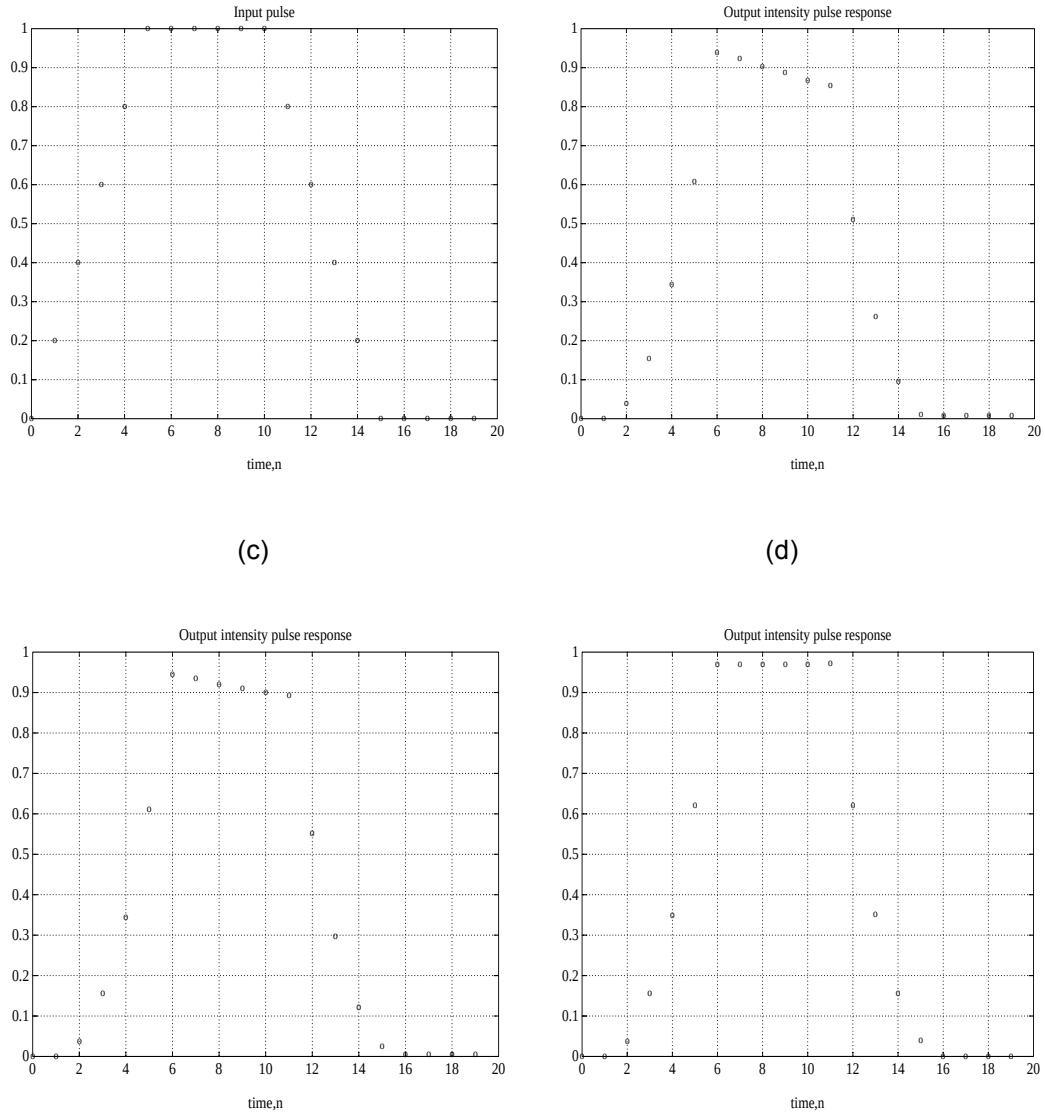

Figure 14 Transient response of the passive DCDR circuit with t_a = 0.99, k = 0.995 and $\omega_o\tau = \pi/2$. (a) Input pulse; (b) Output intensity pulse with π/τ_c = 0.001 (monochromatic); (c) Output intensity pulse with π/τ_c = 0.2; and (d) Output intensity pulse with π/τ_c = 500 (temporal incoherent)

The circuit responses are computed with the same input pulse shape as in *Figure 14*(a), but the circuit parameters here are different. The values of t_a and *k* still satisfy the resonant condition (19) but non-resonant values of $\omega_o\tau$ have been used in (b) and (d). Also, effects of different degree of source coherence on the response are compared. It can be seen in *Figure 15*(a) and (b) that the responses oscillate. The output in (a) which satisfies the resonant condition oscillates more than that in (b). This is because at resonant condition there are many circulating fields in the circuit and they interact with each others. Consider the geometry of our DCDR circuit which have two forward paths and the signals in them

add up at coupler 2 after each circulation. There may not always have constructive interference occurred due to the relative magnitudes of the two beams and their 'signs'. The 'signs' are determined by the phase change the signal experienced when travelling. For instance, after travelling along a fibre path whose $\omega_0\tau$ is denoted by $\pi/2$, this is equivalent to multiplying the complex magnitude of the signal by j which represents the phase. In the case of (a), it may suggest that there are alternating constructive and destructive interference at each circulation that results the oscillations in the output response. In (b), there are less circulating fields taking part in the interaction as most of them travel only once inside the circuit and are out to the output directly. This explains why the average output intensity is larger in (b). The same reasoning can be applied to explain the difference between *Figure 14*(c) and *Figure 15*(a). In the former one, since the value of k is close to 1, most of the beams are coupled out of the circuit after they have travelled only one path in the circuit leaving less amount of circulating beams interacted with incoming beams. Thus the former one does not have oscillation in the output response.

When we increase the value of τ/τ_c to 10 (i.e. decrease in the source coherence length) in Figure 15(c) and (d), the oscillations cease. In this case, the phase change in each fibre path becomes less pronounced since the signals inside the circuit are more incoherent. As a consequence of this, the interference around the path each time would be of the same sign (like a recirculating delay line). Therefore, the output responses are more stable than that in (a) and (b).

(a) (b)

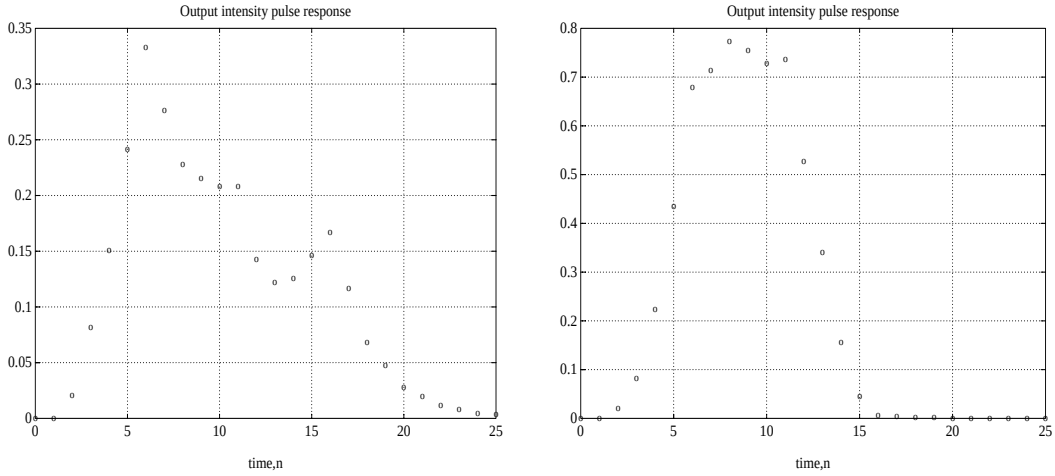

(c) (d)

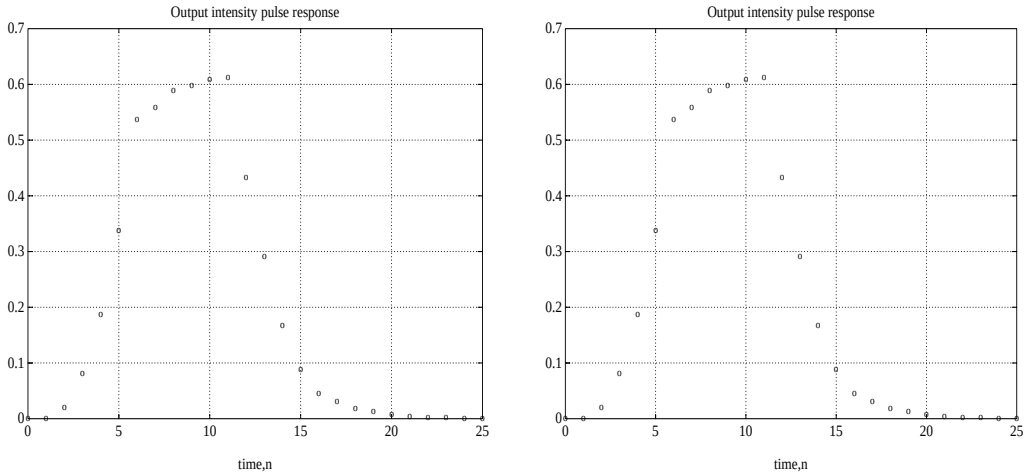

Figure 15 Transient response of the passive DCDR circuit with t_a = 0.8 and k = 0.9. (a) Output intensity pulse with $\omega_0\tau = \pi/2$ and τ/τ_c = 0.2; (b) Output intensity pulse with $\omega_0\tau = \pi$ and τ/τ_c = 0.2; (c) Output intensity pulse with $\omega_0\tau = \pi/2$ and τ/τ_c = 10; and (d) Output intensity pulse with $\omega_0\tau = \pi$ and τ/τ_c = 10.

In *Figure 16*, the effect of source coherence is again shown with an input pulse of the shape as given in Fig. 4.8(a). The most coherent one has the largest oscillation and it is interesting to see that the response has large oscillation even at time after the input pulse cease completely. Generally, a less coherent source results in a less oscillating output response.

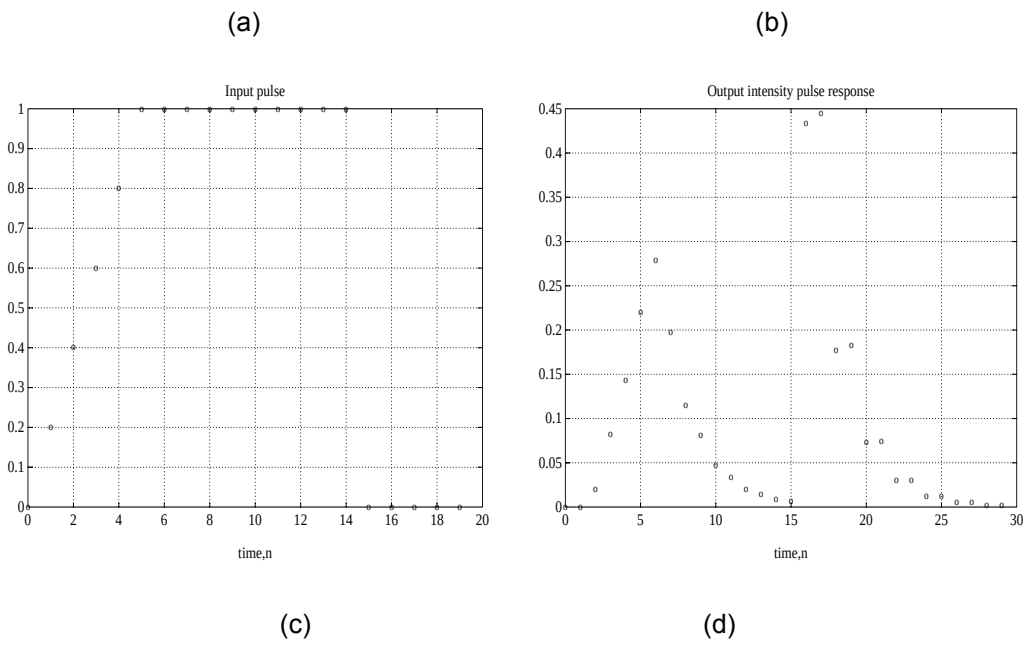

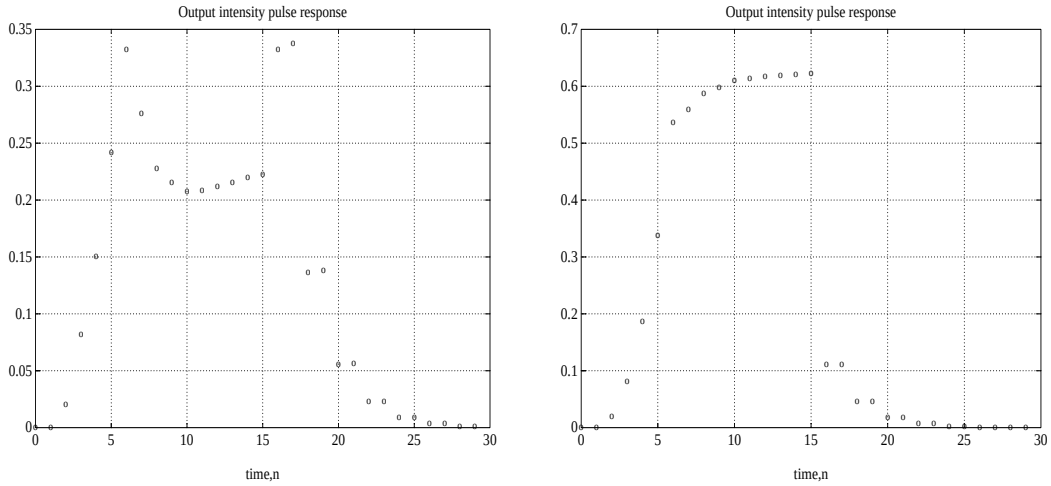

Figure 16 Transient response of the passive DCDR circuit with t_a = 0.8, k = 0.9 and $\omega_o \tau = \pi/2$; (a) Input pulse; (b) Output intensity pulse with τ/τ_c = 0.001; (c) Output intensity pulse with τ/τ_c = 0.2; and (d) Output intensity pulse with τ/τ_c = 10.

The resonant conditions of the DCDR are found and the corresponding behaviour is examined. For the transient response, we have found that the response is oscillatory for source with higher degree of coherence. The results are explained in terms of the interferences among circulating beams in the circuit. The procedures of computation of the transient response is programmed which provides the possibility of analysing other photonic circuits.

3 Fiber dispersion and compensation using DCDR

3.1 Pulse Transmission in Single-mode Optical Fibres

Since the optical fibre is a dispersive medium, an optical pulse broadens as it travels along a fibre. If several pulses are transmitted through the fibre, the broadening of the optical pulse will cause the overlapping among the pulses after travelling a long distance. This interference between adjacent pulses is called the inter-symbol interference (ISI). The ISI will affect the signals received at the other end of the fibre which causes errors in the receiver. The fibre dispersion thus limits the information-carrying capacity of the fibre system as adjacent signal pulses cannot be transmitted too close to each other hence lowering the rate of transmission.

The dominant dispersion mechanism of pulse spreading in single mode fibres (SMF) is the chromatic dispersion which is considered in the following analysis. Chromatic dispersion is mainly due to the wavelength dependence of the refractive index of the fibre's core material and the effects of the waveguide structure that enforce the group velocity of the propagation constant. Furthermore there is

also the polarisation mode dispersion (PMD) generated due to the modal delay of the random variation of the birefringence of the core and cladding of the SMF. This effect will be dealt with in a future report.

The main aim of this section is to obtain the signal at the output of the fibre link so that design of equalizer can be synthesised. As this section is mainly devoted to the study of equalization of fibre dispersion by the DCDR circuit, the discussion on pulse propagation is more specific rather than general. Gaussian pulses are considered.

3.2 Gaussian Pulses and Dispoersion

In this section, the signal at the output of a fibre link is derived that is then used as the input source into the dispersion compensator connected at the end of the fibre link for dispersion equalization. Starting with the signal entering the fibre, that is, the light source, we assume that the light source emits optical signals of Gaussian spectrum centred at $\omega = \omega_o$ as:

$$S(\omega) = \frac{\sqrt{2\pi}}{W_s}\exp[-(\omega?\omega_o)^2/(2W_S^2)] \qquad (44)$$

where W_S is the spectral FWHM width in units of angular frequency ω is the angular optical frequency and ω_o is the centre angular frequency of the source. The corresponding temporal (time domain) function $s(t)$, by applying the Fourier transform on (44), is

$$s(t) = e^{\frac{-t^2 W_s^2}{2}} e^{j\omega_0 t} \qquad (45)$$

The the light source signal is externally modulated. Suppose the source is amplitude modulated with a pulse of Gaussian shape of the form:

$$A_m(t) = e^{\left(\frac{-t^2}{2\tau_m^2}\right)} \qquad (46)$$

where τ_m is the 1/e half width. Thus, the light signal, or the electric field of the input waves, $E_{if}(t)$ can be expressed as:

$$E_{if} = A_m s(t) \qquad (47)$$

i.e. $$E_{if}(t) = e^{\left[\frac{-t^2}{2}\left(\frac{1}{\tau_m^2}+W_s^2\right)\right]} e^{j\omega_0 t} \quad (48)$$

The electric field at the end of the fibre of length L is

$$E_{of}(t) = \int \mathrm{E}_{if}(\omega)\exp[j(\omega t - \beta L)]d\omega \quad (49)$$

where $E_{if}(\omega)$ is the Fourier transform of $E_{if}(t)$, β is the propagation constant of the propagation mode in the fibre. Low-loss fibre is assumed to be used so that attenuation of the fibre can be neglected. The dispersion effect of the fibre can be represented by the fact that β is a function of frequency. By Taylor's series expansion of β about $\omega = \omega_0$, β can be approximated by

$$\beta(\omega) = \beta(\omega_o) + \beta'(\omega_o)(\omega - \omega_o) + \frac{\beta''(\omega_o)}{2}(\omega - \omega_o)^2 + \ldots \quad (50)$$

For simplicity, we use β_0 to represent $\beta(\omega_0)$ for the rest of this report. In the following analysis, only the terms up to the second derivative of the propagation constant are included. The higher-order derivative terms in the Taylor series expansion of the propagation constant are neglected. Moreover, the first two terms in (40) represent the pure delay of the carrier and the envelope respectively and they do not contribute to the dispersion. The effective propagation constant used in our analysis can then be represented by

$$\beta(\omega) = \frac{\beta_o''}{2}(\omega - \omega_o)^2 \quad (51)$$

The value of the second derivative of the propagation constant is a measure of the so-called first order dispersion[3.1,3.2]. For a silica fibre, the wavelength at which this first order dispersion vanishes is about 1300nm. At wavelength other than the zero-dispersion wavelength, the first-order dispersion is non-zero and it accounts for the broadening of optical pulse travelling in the fibre. Also, the values of higher order of derivatives which correspond to second- and higher-order dispersion are negligible at wavelength other than the zero-dispersion wavelength.

By using (39) and (41), from reference [3.1, 3.2], the output power at the fibre end is

$$I_{of}(t) = \frac{1}{[1+4\hat{D}^2(1+V^2)]^{1/2}} \exp\left[\frac{-(t/\tau_m)^2}{1+4\hat{D}^2(1+V^2)}\right] \quad (52)$$

with $V = \omega_m W_S$, (53)

$$\hat{D} = \frac{\beta_o'' L}{2\tau_m^2} \quad (54)$$

(54) shows that the Gaussian shape pulse remains Gaussian after travelling through the fibre. It can also be stated that the output power at the fibre end has a pulse width τ_o which is given by:

$$\tau_o^2 = \tau_m^2(1+4\hat{D}^2(1+V^2) \quad (55)$$

This clearly shows that a larger value of V would produce a larger pulse width τ_o at the fibre output end. From (55), this means an incoherent source (large W_S) broadens the signals more than the case with a coherent source (small W_S). Moreover, the broadening of pulses depends on the value of $\hat{D}$, hence the values of β_o'' and L.

Without loss of generality, the source is assumed to be monochromatic in the following analysis, i.e. W_S = 0. This makes V = 0. From reference [3.1, 3.2], the electric field at the fibre output for a monochromatic light source is given by:

$$E_{of}(t) = \frac{1}{\left(1+4\hat{D}^2\right)^{1/4}} \exp(j\omega_o t) \exp\left[\frac{-(t/\tau_m^2)}{2(1+4\hat{D}^2)}\right] \exp\left[\frac{-j\hat{D}(t/\tau_m^2)}{(1+4\hat{D}^2)}\right] \quad (56)$$

Expressing (56) in terms of the physical parameters, resulting:

$$E_{of}(t) = \frac{\tau_m}{\left[\tau_m^4 + (\beta_o'' L)^2\right]^{1/4}} \exp(j\omega_o t) \exp\left\{\frac{-t^2(\tau_m^2 + j\beta_o'' L)}{2[\tau_m^4 + (\beta_o'' L)^2]}\right\} \quad (57)$$

which is the same expression as obtained in [3.10]. This is the lightwave field at the input of the compensator.

3.3 Single mode fibre propagation

In this section, we investigate the application of the DCDR circuit as an equalizer for single mode fibre dispersion. The principle of the fibre dispersion equalizer lies in the fact that the equalizer has a group delay in the opposite sign to that introduced by the fibre. Thus the group delay induced on the signal after the signal travels through the fibre would be partially or completely cancelled by that in the equalizer. Recall that the magnitude of the phase change induced by the fibre on the signal after the signal travels length L of fibre is βL. Thus, the group delay time τ_f induced by the fibre can be expressed as:

$$\tau_f = \beta_o''(\omega-\omega_0)L \tag{58}$$

which is obtained by differentiating βL with respect to ω. The chromatic dispersion induced by the fibre link of length L is thus equal to

$$\frac{d\tau_f}{d\omega} = \beta_o'' L \tag{59}$$

Ideally, we need to use the linear portion of the equalizer group delay that has the suitable slope, both the magnitude and the sign, to counteract the fibre dispersion. In addition, that portion should be positioned to the centre frequency of the signal. This point is called the operating point of the equalizer thereafter.

Firstly, we consider the pulse at the fibre link output whose field equation is given in (57). The following parameters are used in our analysis. The input pulse into the fibre is a Gaussian shaped pulse with temporal half width at the 1/*e* points and τ_m equals to 50ps. The working wavelength of the system, λ_o, is taken to be 1550nm in the following analysis. As we only concentrate on the dispersive effect of the fibre, the attenuation effect of the fibre is ignored. Therefore, the fibre is assumed to be lossless. As the operating wavelength of the system is 1550 nm at which the loss of standard fibre is at minimum, the above assumption is valid. Actually the attenuation introduced by the fibre can be easily compensated by an amplifier or repeater at the end of the fibre length but this is not the main point in our analysis. The fibre dispersion value is represented by a parameter D which is 17ps/nm/km for conventional silica fibre. The dispersion caused by fibre is given by $\beta_o'' L$ (59) which is

$$\beta_o'' L = \frac{D\lambda_o^2 \mathrm{L}}{2\pi C} \tag{60}$$

where *C* is the speed of light in vacuum. The transmission fibre path length *L* is taken to be 200 km unless otherwise stated. Using the given parameters, the value of $\beta_o'' L$ is 4.3335e^{-21}. The intensities of the optical pulses at the input of the fibre and at the fibre output with the above fibre parameters and operating conditions are plotted in ***Figure 17***. The dispersive properties of the fibre can be clearly observed when the difference between the pulse widths of the two pulses is compared. Obviously, the optical pulse broadens as it travels along the fibre.

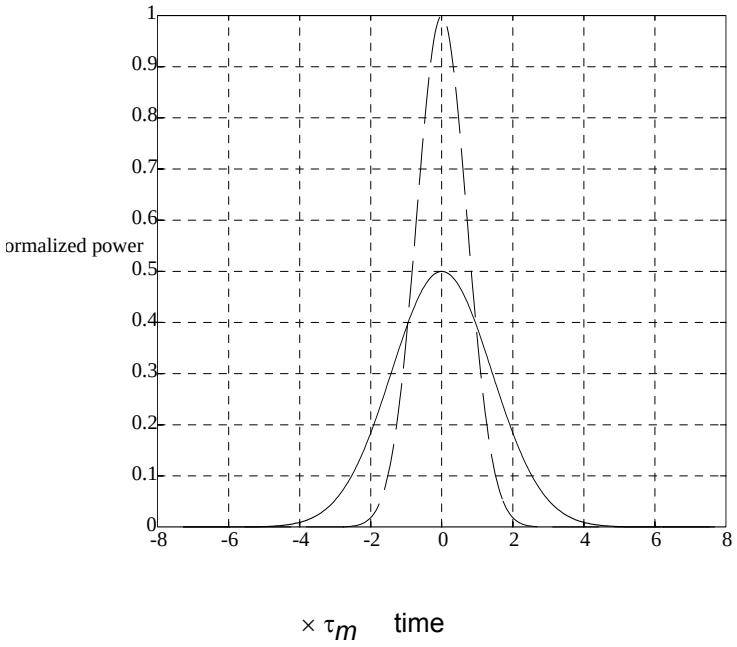

Figure 17 Intensities of the optical pulses at the input of the fibre (dotted line) and at the fibre output (solid line) with the above fibre parameters and operating conditions.

4 Dispersion Compensation by the Photonic Circuit

The performance of optical communication systems can be limited by several effects. One of these effects is the pulse distortion due to fibre chromatic dispersion. The study of pulse propagation in dispersive media is important in many applications, including the transmission of optical pulses through the optical fibres [3.1-3.6] used in optical communication systems [3.7-3.9]. In the fibre-optic transmission system, compensators or dispersion equalizers [3.10-3.13] are required to compensate for the distortion resulted during the signal transmission in the fibre. This ensures that the signal distortion at the end of the transmission link is kept to the minimum so that the signal is received without error. In this section, the possibility of employing the DCDR resonator as a dispersion equalizer is investigated.

In the first part of this section, the equations governing the optical pulse transmission in single mode fibre are derived. These equations will include the effects of source coherence and the modulation signal bandwidth on the pulse broadening behaviour in the fibre. The application of DCDR circuit as the dispersion equalizer is studied in the second part of this section.

4.1 Group delay and dispersion of the DCDR resonator

The group delay and the dispersion of the DCDR resonator is evaluated numerically using programs written in Matlab commands. Recall that τ is the basic delay time of the DCDR circuit and it is set to the value of 20ps which is equal to $\tau_m/2.5$. One result is shown in ***Figure 18*** with $k_1 = k_2 = 0.1$, $t_{a1} = t_{a2} = t_{a3} = 1$, $G_1 = G_2 = G_3 = -1$ and $m_1 = m_2 = m_3 = 1$.

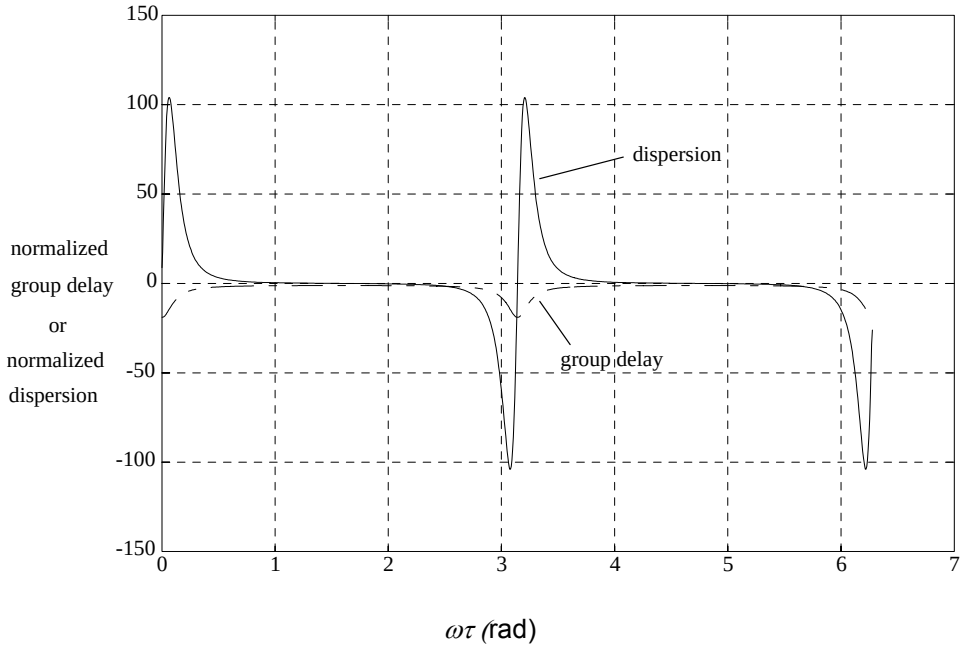

Figure 18 Group delay (-.-.-) and dispersion (solid line) of the resonator with $k_1 = k_2 = 0.1$, $t_{a1} = t_{a2} = t_{a3} = 1$, $G_1 = G_2 = G_3 = -1$ and $m_1 = m_2 = m_3 = 1$. Since the group delay and dispersion values are normalized, the group delay value read on the axis needed to be multiplied by τ to deduce the absolute value. This is to be multiplied by τ^2 for the dispersion factor.

It is found in ***Figure 18*** that the group delay of the equalizer is always negative while its dispersion has both positive and negative values. The negative portion of the equalizer dispersion can be employed to cancel the effect of fibre dispersion.

4.2 Compensation

The task of the DCDR circuit is to compensate the linear induced dispersion generated by the fibre transmission line. Let the ratio of equalizer dispersion to the fibre dispersion be *R*, the ideal value of *R* would then be -1. We also need to choose the operating point of the equalizer so that we can get the desired equalizer dispersion to perform the equalization. The operating point of the equalizer, ϕ_O, is actually the operating $\omega\tau$ of the DCDR circuit. The operating point can be positioned by changing the length of the fibre path in the DCDR circuit piezoelectrically. In order to get better equalization, the equalizer dispersion should vary as small as possible with $\omega\tau$ in the vicinity of ϕ_O. This is due to the fact that we have assumed constant fibre dispersion (dispersion slope is negligible over the considered spectral range) in the vicinity of the source operating wavelength. The value of ϕ_O can be chosen from the resonator dispersion in ***Figure 2***. It is found that at $\omega\tau_\mu$= 2.8225 rad , the magnitude of the equalizer dispersion is 4.3617e^{-21} which gives a *R* of -1.0065. The corresponding output intensity of the equalizer together with the input intensities of the fibre and equalizer are shown in *Figure 19*.

By the comparison between the resonator input intensity and the resonator output intensity in *Figure 19*, it can be seen that the broadening of the former pulse has been compensated to a great extent by the resonator. The resonator cannot give full equalization because its dispersion is not constant with frequency. For that reason, we attempt to design parameters giving the best rather than 100% equalization for a given pulse. The loss in the magnitude of the equalized pulse can be compensated by an amplifier inserted after the resonator.

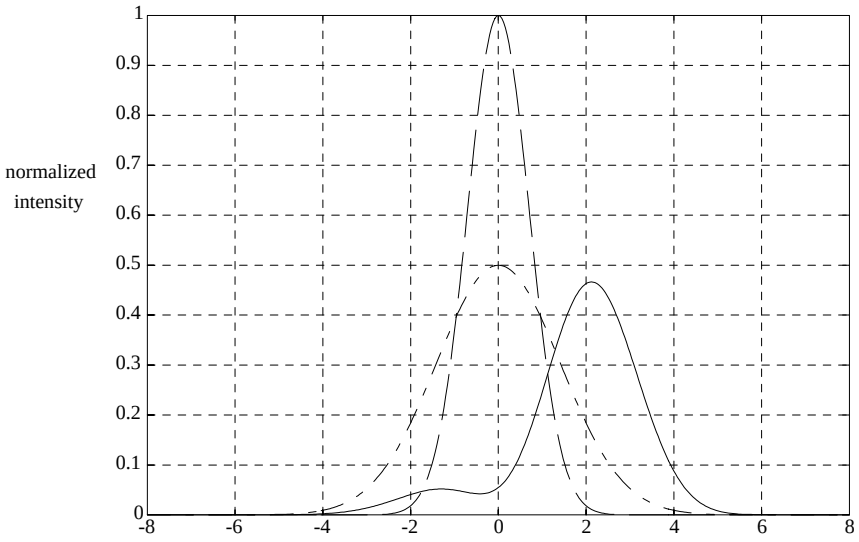

$\times \tau_m$ time

Figure 19 The intensities of the optical pulses at the input of the fibre (dashed ---), at the fibre output (i.e. resonator input) (dashdot -·-) and at the resonator output (solid line) with $k_1 = k_2 = 0.1$, $t_{a1} = t_{a2} = t_{a3} = 1$, $G_1 = G_2 = G_3 = 1$ and $m_1 = m_2 = m_3 = 1$, operating point of the resonator $\phi_0 = 2.8225$ rad (161.7°).

The effects of different operating points on the equalization are shown in ***Figure 20***. The operating points are indicated in the figure.

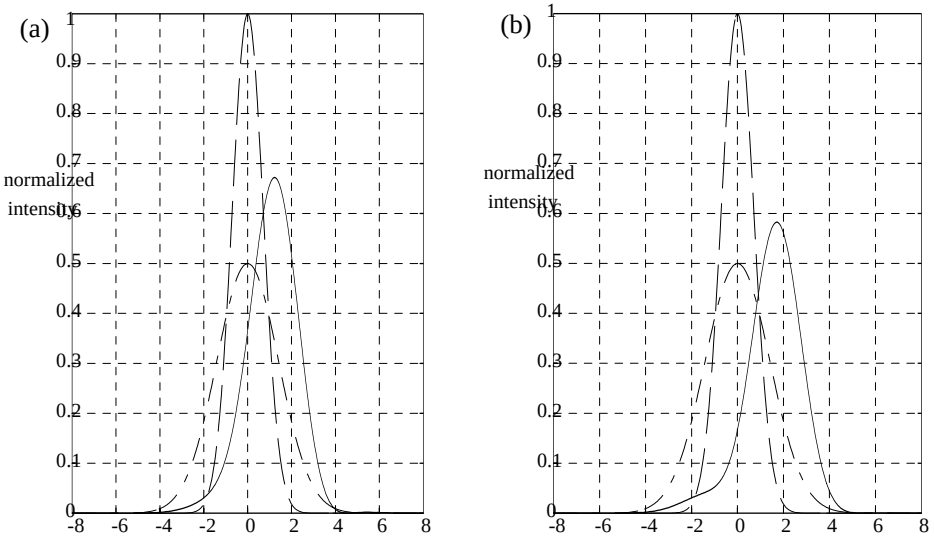

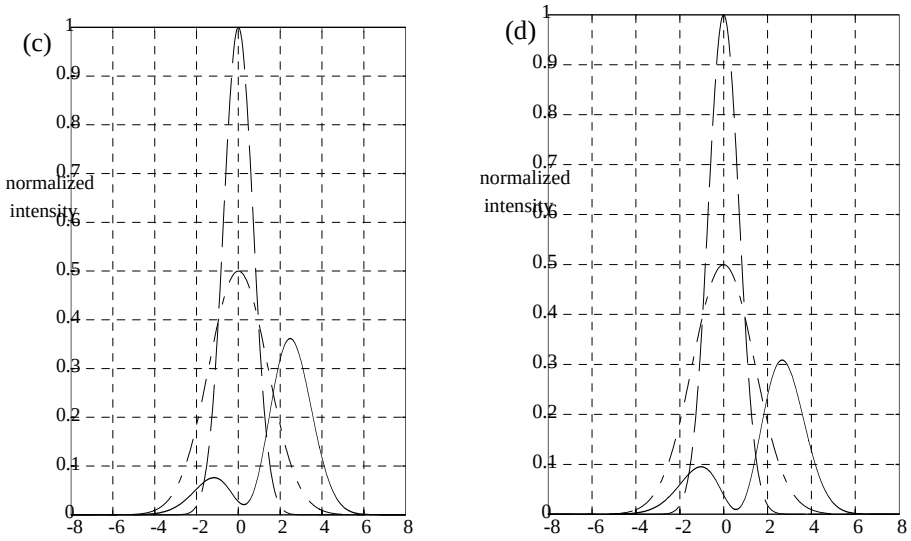

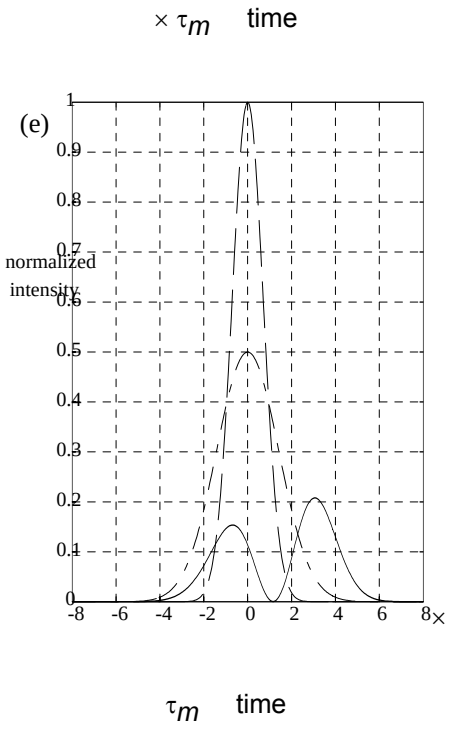

Figure 20 The intensities of the optical pulses at the input of the fibre (dashed ??), at the fibre output (i.e. resonator input) (dashdot --) and at the resonator output (solid line) with $k_1 = k_2 = 0.1$, $t_{a1} = t_{a2} = t_{a3} = 1$, $G_1 = G_2 = G_3$=-1 and $m_1 = m_2 = m_3 = 1$ for different operating points of the resonator. (a) ϕ_o = 2.5035 rad, (b) ϕ_o = 2.6814 rad, (c) ϕ_o = 2.9391 rad, (d) ϕ_o = 3.0005 rad, and (e) ϕ_o = 3.1355 rad.

The operating points for the plots in *Figure 20* are all in the proximity of ϕ_o = 2.8225 rad, i.e. the operating point used in *Figure 19*. In this range of ϕ_o, the resonator's dispersion is negative which is appropriate for its use as an equalizer. It can be observed that when we moves from the operating point ϕ_o = 2.5035 to ϕ_o = 3.1355, a trailing tail of the signal is building up. It becomes significant as compared to the original signal thus causing another distortion. Therefore, the phase values ϕ_o in *Figure 20*(c)-(e) are not good operating points for equalisation.

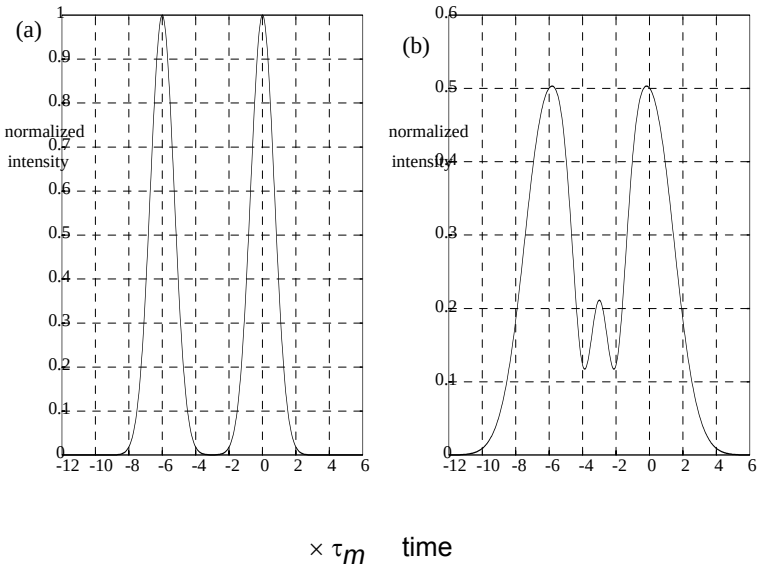

Figure 21 Two adjacent pulses (a) at the input of the fibre link and (b) at the end of the fibre link before the equalizer. The two pulses are separated $6\omega_m$ in time.

To visualise the effect of broadened pulses, we consider a sequence of pulses. *Figure 21*(b) shows the overlapping between two adjacent pulses separated $6\omega_m$ in time at the end of the fibre link after undergoing dispersion. *Figure 21*(a) shows that the two pulses were originally with no interference between them at the transmitted end. If the sampling time of the detection system is $6\omega_m$ in this situation, the fibre dispersion would not cause any problem to the detection. But if the pulses are getting closer to each others, i.e. at a higher transmission rate, the ISI would limit the capacity of the system.

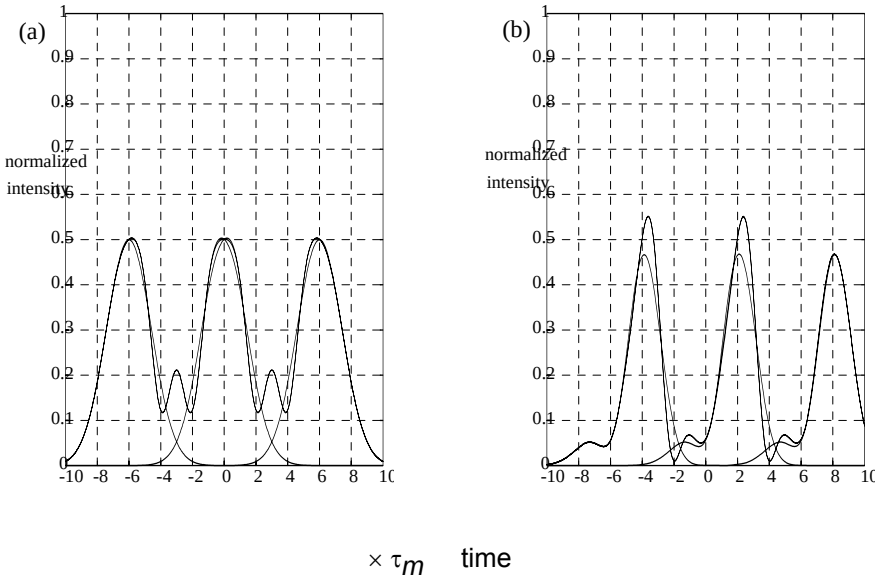

Figure 22 (a) The eye pattern diagram before the equalizer, (b) the eye pattern diagram after the equalizer. The parameters used in the equalizer are the same as that used in Figure 21. Pulses are separated by $6\tau_m$ in time.

The eye pattern diagram is normally used to assess the system performance in digital communication systems. Firstly, random data signal patterns (PRBS) are generated. When the PRBS combinations are superimposed simultaneously, an eye pattern diagram is formed. The eye pattern diagrams of the optical wave intensities at pre- and post- equalizer are shown in *Figure 22*(a) and (b) respectively. Recall that the operating point of the equalizer here is 2.8225 rad. It is noted in *Figure 22*(b) that the eye opening of the diagram is greater than that in Fig. *Figure 22*(a), thus the equalizer has indeed improves the bit-error-rate (BER). In *Figure 23*, the eye diagrams for two different transmission rates are shown. In *Figure 23*(a), the pulses are pushed closer together, and the time between their adjacent peaks is $4\tau_m$. The corresponding time is $8\tau_m$ in *Figure 23*(b). It is obvious that the eye closure in *Figure 23*(a) is greater than that in *Figure 23*(b). This means that it is more difficult to detect signal correctly in the case of *Figure 23*(a). By comparing among the eye diagrams in *Figure 22* and *Figure 23*, we can state that the minimum spacing between transmitted pulses is about $6\omega_m$ in this instance. This, in turn, is a way of determining the maximum transmission rate of a transmission channel.

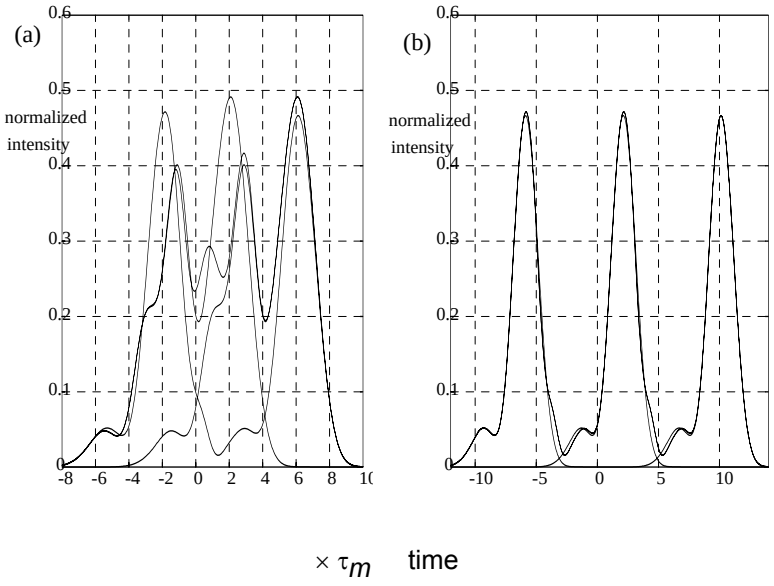

Figure 23 Eye pattern diagrams after the equalizer. The parameters used in the equalizer are the same as that used inFigure 22 (a) Pulses are separated by $4\tau_m$ in time; (b) pulses are separated by $8\tau_m$ in time.

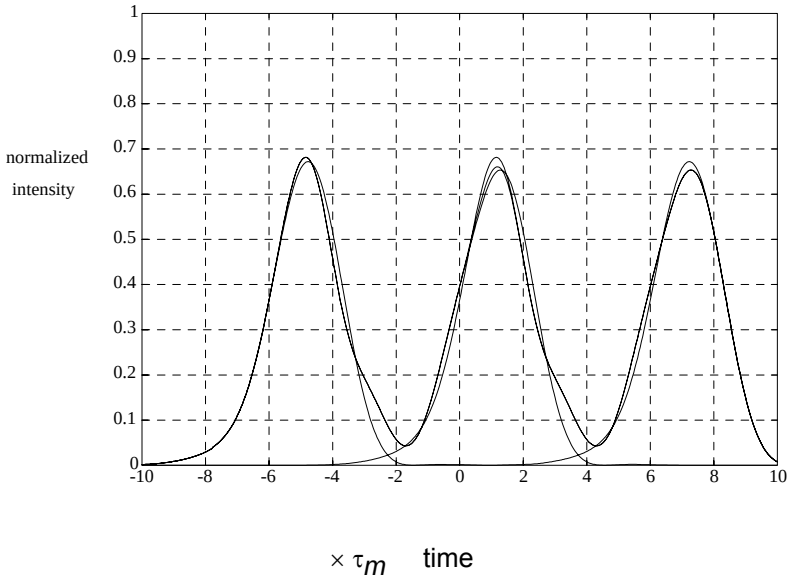

Figure 24 Eye pattern diagrams after the equalizer. The parameters used in the equalizer are the same as that used in Figure 19 except that ϕ_0 = 2.5035 rad. Pulses are separated by 6 τ_m in time.

In *Figure 24*, we have shown that with ϕ_0 = *2.5035 rad* and *R = -0.1473*, the result is even better than that in *Figure 22* with ϕ_0 = *2.8225* rad and R = -1.0065. These results show that the DCDR resonator can be used as an equalizer even in the passive operation. Since the dispersion of equalizer is proportional to ω^2, it is expected that a larger value of τ would result in a greater magnitude of the equalizer dispersion. In *Figure 25*, two values of τ are used with the same operating point ϕ_0 = *2.5035 rad*. It can be seen that a better compensation is obtained by the equalizer with a larger τ.

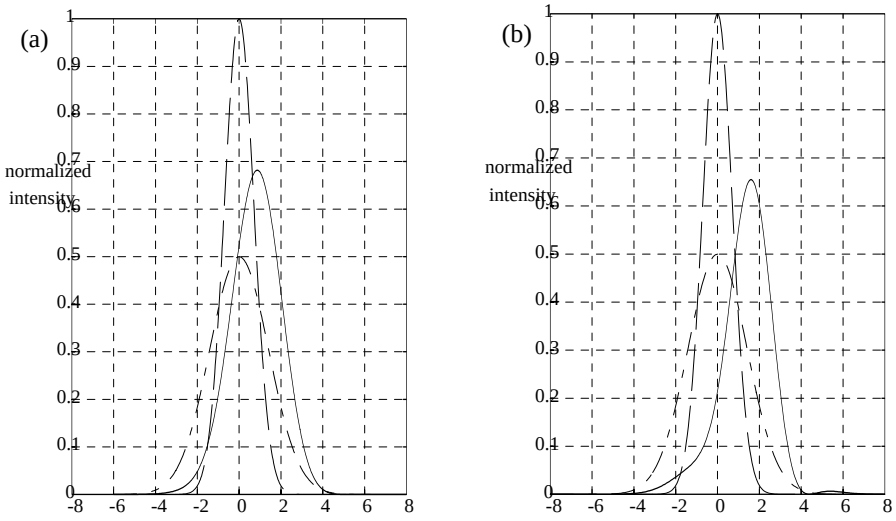

$\times \tau_m$ time

Figure 25 The intensities of the optical pulses at the input of the fibre (dashed --), at the fibre output (i.e. resonator input) (dashdot-.-) and at the resonator output (solid line) with $k_1 = k_2 = 0.1$, $t_{a1} = t_{a2} = t_{a3} = 1$, $G_1 = G_2 = G_3 = 1$ and $m_1 = m_2 = m_3 = 1$, operating point of the resonator ϕ_0 = 2.5035 rad. (a) τ = 15ps, and (b) τ = 25ps.

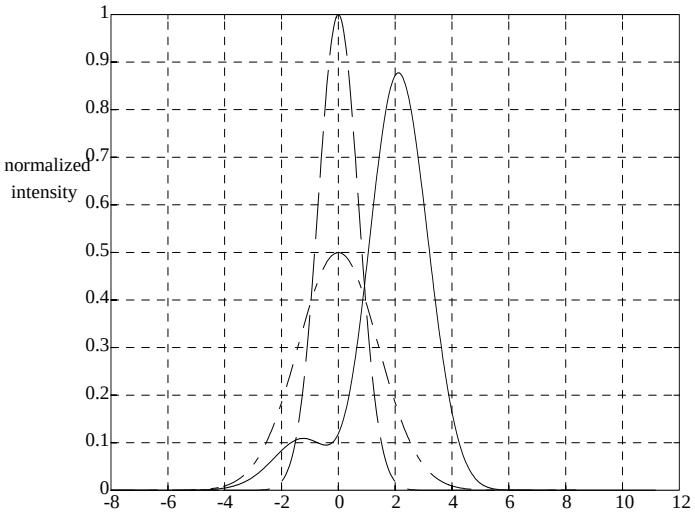

$\times \tau_m$ time

Figure 26 The intensities of the optical pulses at the input of the fibre (dashed --), at the fibre output (i.e. resonator input) (dashdot-.-) and at the resonator output (solid line) with $k_1 = k_2 = 0.1$, $t_{a1} = t_{a2} = t_{a3} = 1$, $G_1 = 1.9$, $G_2 = G_3 = -1$ and $m_1 = m_2 = m_3 = 1$, operating point of the resonator ϕ_0 = 2.8225 rad.

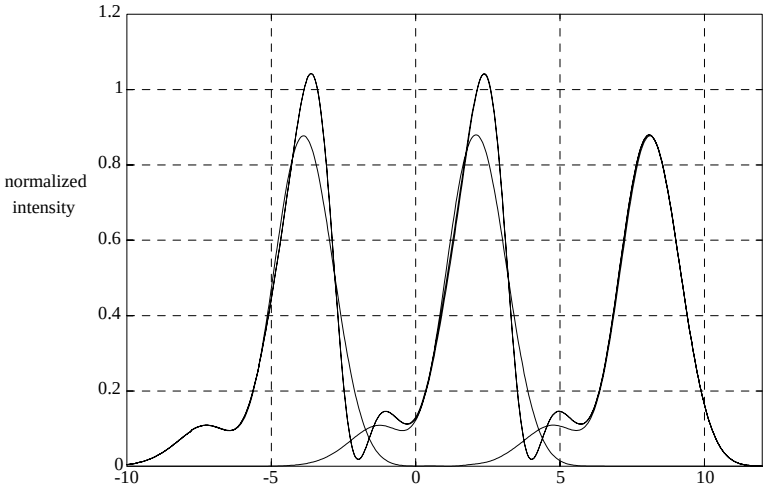

$\times \tau_m$ time

Figure 27 Eye pattern diagram after the equalizer. The parameters used in the equalizer are the same as that used in Figure 19. Pulses are separated by $6\tau_m$ in time.

An active mode operation of the equalizer is shown in *Figure 26*. The parameters used are $k_1 = k_2 = 0.1$, $t_{a1} = t_{a2} = t_{a3} = 1$, $G_1 = 1.9$, $G_2 = G_3 = -1$ and $m_1 = m_2 = m_3 = 1$. The operating point of the resonator is located at *2.8225 rad* which is the same as that in *Figure 24*. The value of *R* in this case is -1.0074. By comparing between *Figure 19* and *Figure 27*, it is obvious that the equalized pulse in the latter graph has a larger magnitude. Thus, the amplifier in the DCDR circuit compensates for the loss in magnitude as well. This is a useful feature in our amplified DCDR circuit as the dispersion compensation and the compensation for the pulse magnitude can be done with a single device. In other words, in addition to the dispersion equalization, the DCDR circuit can be tailored to compensate for the attenuation in the pulse amplitude. This would be an economical way of equalizer design.

The eye diagram for the equalized pulse in *Figure 26* is given in *Figure 27*. The eye diagram before the compensator is the same as that in *Figure 22*(a). The eye diagram in *Figure 27* is compared with that in Fig. *Figure 23*(b) where we have passive mode operation. In both cases, the equalizers have performed considerable amount of dispersion equalization. The simulators have been tested for a single loop resonator using the same parameters as given in Ref[10], and after value-by-value comparison, our results are consistent.

5 Concluding remarks

The application of using the DCDR circuit as a dispersion equalizer is demonstrated. The photonic circuit has been design and synthesized using the photonic signal processing technique. Signal low graph has been described with specific application to the transfer function and the analysis o the amplitude and phase frequency responses. The effects of working the equalizer at several operating points are shown. It is found that the DCDR circuit can provide a reasonable amount of chromatic dispersion equalization. Active operation of the DCDR circuit can provide compensation for the pulse amplitude in addition to the dispersion compensation. Therefore, theoretically, the circuit can be employed as a dispersion equalizer in fibre-optical communication systems.

6 References

[2.1] Y. Ohtsuka, "Analysis of a fiber-optic passive loop-resonator gyroscope : dependence on resonator parameters and light-source coherence"
[2.2] *J. Lightwave Tech.*, vol. LT-3, no.2, pp. 378-384, April 1985.
[2.3] G.F. Levy, " Optical fibre ring resonators: analysis of transient response " *IEE Proceedings-J*, vol.139, No.5, pp. 313-317, October 1992.
[2.4] B. Moslehi, "Analysis of optical phase noise in fiber-optic systems employing a laser source with arbitrary coherence time" *J. Lightwave Tech.*, vol. LT-4, no.9, pp. 1334-1351, Sep 1986.

[2.5] B. Crosignani, A. Yariv, P. Di Porto, "Time-dependent analysis of a fiber-optic passive-loop resonator" *Optics Letters*, vol. 11, no. 4, pp. 251-253, April 1986.
[2.6] K. Petermann, "Semiconductor laser noise in an interferometer system" *IEEE J. Quantum Electronics*, vol. QE-17, no. 7, pp. 1251-1256, July 1981.
[2.7] Y. Ohtsuka, "Optical coherence effects on a fiber-sensing Fabry-Perot interferometer", *Applied Optics*, vol. 21, no. 23, pp. 4316-4320, Dec 1982.
[2.8] LN Binh, *"Photonic Signal Processing - Part I: Analysis and Graphical Representation of Photonic Circuits", Technical Report at* http://www.ds.eng.monash.edu.au/techrep/reports/2005/MECSE-7-2005.pdf

[3.1] D. Marcuse, "Pulse distortion in single-mode fibers," *Applied Optics*, vol. 19, pp. 1653-1660, 1980.
[3.2] D. Marcuse, "Selected topics in the theory of telecommunications fibers," *Optical Fiber Telecommunications II*, Chapter 3, Academic Press, Inc., 1988.
[3.3] B. E. A. Saleh and M. I. Irshid, "Transmission of pulse sequences through monomode fibers," *Applied Optics*, vol. 21, no. 23, pp. 4219-4222, Dec 1982.
[3.4] B. E. A. Saleh and M. I. Irshid, "Coherence and intersymbol interference in digital fiber optic communication systems," *IEEE J. Quantum Electronics*, vol. QE-18, no. 6, pp. 944-951, June 1982.
[3.5] K. Jorgensen, "Transmission of Gaussian pulses through monomode dielectric optical waveguides," *Applied Optics*, vol. 16, no. 1, pp. 22-23, Jan 1977.
[3.6] K. Jorgensen, "Gaussian pulse transmission through monomode fibers, accounting for source linewidth," *Applied Optics*, vol. 17, no. 15, pp. 2412-2415, August 1978.
[3.7] C. Lin and D. Marcuse, "Optimum optical pulse width for high bandwidth single-mode fibre transmission," *Electronic Letters*, vol. 17, no. 1, pp. 54-55, Jan 1981.
[3.8] D. Marcuse and C. Lin, "Low dispersion single-mode fiber transmission - the question of practical versus theoretical maximum transmission bandwidth," *IEEE J. Quantum Electronics*, vol. QE-17, no. 6, pp. 869-878, June 1981.
[3.9] P. M. Shankar, "Performance of LED/single mode fiberoptic systems," J. Opt. Commun., 10(1989) 4, pp. 132-137.
[3.10] S. Dilwali and G. Soundra Pandian, " Pulse response of a fiber dispersion equalizing scheme based on an optical resonator ", *IEEE Photonics Technology Letters*, vol.4, no.8, pp.942-944, Aug 1992.
[3.11] K. Iwashita and N. Takachio, "Chromatic dispersion compensation in coherent optical communications," *J. Lightwave Technology*, vol. 8, no. 3, pp. 367-375, March 1990.
[3.12] L. J. Cimini, Jr., L. J. Greenstein and A. A. M. Saleh, "Optical equalization to combat the effects of laser chirp and fiber dispersion," *J. Lightwave Technology*, vol. 8, no. 5, pp. 649-659, May 1990.
[3.13] S. D. Personick, "Comparison of equalizing and nonequalizing repeaters for optical fibe systems," *Bell System Technical Journal*, vol. 55, no. 7, pp. 957-971, Sep 1976.
[3.14] S. Kitajima, N. Kikuchi, K. Kuboki, H. Tsushima, and S. Sasaki, "Dispersion compensation with optical ring resonator in coherent optical transmission systems," *International Conf. on Integrated Optics and Optical Communications*, pp. 353-356, San Francisco, 1993.
[3.15] L.N. Binh, „ Photonic Singa processing – Part I: Anaysis and Graphical representation of photonic circuits", Technical report No. MECSE-7-2005, Department of Eectrica and Computer Systems Engineering, Monash University, URL: http://www.ds.eng.monash.edu.au/techrep/reports/2005/MECSE-7-2005.pdf.